A Ruthenium Hydrido Dinitrogen Core Conserved Across Multielectron/Multiproton Changes to the Pincer Ligand Backbone

Quinton J. Bruch,[†] *Brian M. Lindley,*[†] *Bjorn Askevold,*[‡] *Sven Schneider,*[‡] *Alexander J. M. Miller*[†]*

[†] Department of Chemistry, University of North Carolina at Chapel Hill, Chapel Hill, North Carolina 27599-3290, United States

[‡] University of Goettingen, Institute for Inorganic Chemistry, 37077 Goettingen, Germany

*Corresponding Authors Email Address: ajmm@email.unc.edu

ABSTRACT. A series of ruthenium(II) hydrido dinitrogen complexes supported by pincer ligands in different formal oxidation states has been prepared and characterized. Treating a ruthenium dichloride complex supported by the pincer ligand bis(di-*tert*-butylphosphinoethyl)amine (H-PNP) with reductant or base generates new five-coordinate *cis*-hydridodinitrogen ruthenium complexes each containing different forms of the pincer ligand. Further ligand transformations provide access to the first isostructural set of complexes featuring all six different forms of the pincer ligand. The conserved *cis*-hydridodinitrogen structure facilitates characterization of the π–donor, π–acceptor, and/or σ–donor properties of the ligands and assessment of the impact of ligand-centered multielectron/multiproton changes on N_2 activation. Crystallographic studies, infrared spectroscopy, and ^{15}N NMR spectroscopy indicate that N_2 remains weakly activated in all cases, providing insight into the donor properties of the different pincer ligand states. Ramifications on applications of (pincer)Ru species in catalysis are considered.

Introduction

Dinitrogen coordination to a transition metal was first observed in the ruthenium ammine complexes $[Ru(NH_3)_5(N_2)]^{2+}$ and $[(NH_3)_5Ru(\mu\text{-}N_2)Ru(NH_3)_5]^{4+}$,[1,2] ushering in a wave of coordination chemistry and catalysis.[3–5] Upon binding to a transition metal, N_2 undergoes some degree of "activation" or weakening of the N–N bond. The extent of N_2 activation is typically assessed by X-ray crystallography or infrared (IR) spectroscopy (Scheme 1).[3,6,7] Crystallographic studies can provide information on the N_2 bond order; the triple bond of free N_2 is 1.10 Å,[8] and elongation to 1.15 Å is considered indicative of a singly reduced dinitrogen ligand.[8] IR spectroscopy reports on N_2 activation via the N–N stretching frequency, ν_{NN}. Upon binding of N_2 to one transition metal ion, a large shift in ν_{NN} to lower frequency is observed with ν_{NN} of terminal M–N_2 existing over a range of 1850-2200 cm^{-1}.[8,9] Terminal N_2 complexes of Mo (ν_{NN} = 1859 cm^{-1}),[9] Fe (ν_{NN} = 1920 cm^{-1}),[10,11] Ru (ν_{NN} = 1960 cm^{-1}),[12] and Os (ν_{NN} = 1931 cm^{-1})[12] with low energy stretching frequencies indicative of activated N_2 have shown activity for catalytic NH_3 production.

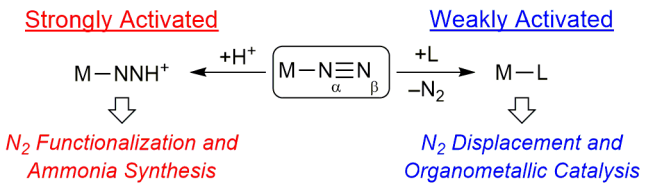

Scheme 1. Categorization of transition metal N_2 complexes.

As shown in Scheme 1, strongly activated N_2 ligands have been a starting point for molecular approaches to N_2 functionalization,[4,13–15] whereas complexes bearing weakly activated N_2 ligands have shown promise as precatalysts for organometallic transformations.[16–19] In

precatalysts, the N_2 ligand can stabilize highly reactive, low-coordinate and low-valence-electron species, but is often sufficiently labile to enable high catalytic activity via facile substrate binding. A number of pincer ruthenium dinitrogen and hydrido dinitrogen complexes have been shown to catalyze ketone transfer hydrogenation[20,21] and acceptorless dehydrogenation of alcohols.[18,19,22]

Ruthenium metal is also a heterogeneous catalyst for N_2 hydrogenation in the Kellogg Advanced Ammonia Process (as well as the reverse process of ammonia oxidation).[23,24] Recent work has shown that molecular ruthenium and osmium complexes are capable of catalytic N_2 fixation and N_2 bond cleavage.[12,25] Computational studies have suggested that ruthenium pincer complexes may also be viable catalysts for N_2 conversion, particularly with the aid of metal-ligand cooperation.[26] In fact, experimental studies have demonstrated that ruthenium complexes supported by the ligand $N(CH_2CH_2P^tBu_2)_2^-$ (PNP) can support key steps relevant to ammonia synthesis.[27,28] For example, the nitride (PNP)Ru(N) is converted to free ammonia by a hydrogenation that involves metal-ligand cooperative H_2 activation (Scheme 2).[27] A separate ligand-assisted mechanism for ammonia synthesis is accessed upon addition of an appropriate ligating acid to the amine-backbone variant $[(H\text{-}PNP)Ru(N)]^+$ (Scheme 2).[28] Protonation of this cationic nitride induces a metal-ligand cooperative proton-coupled electron transfer to produce the ammonia-bound complex $[(PC{=}NP)Ru(NH_3)(O_2CAr')]^+$ (Ar' = 4-methoxyphenyl, see Scheme 3 below for ligand abbreviations). However, the parent nitrides have not been formed directly from N_2, motivating studies into whether (pincer)Ru complexes might bind and activate dinitrogen upon reduction. Though N_2 cleavage remains rare, photochemical cleavage $[(NH_3)_5Os^{II}(\mu\text{-}N_2)Os^{III}(NH_3)_5]^{5+}$ has resulted in a N_2-derived terminal nitride at a Group 8 metal.[25]

In preliminary studies, we targeted reduction of $[(PC{=}NP)Ru(NH_3)(O_2CAr')]^+$ (Scheme 2) to induce NH_3 release and uptake of N_2. Reductive electrolysis of the ammine complex produced a mixture of several hydride-containing products tentatively postulated to be dinitrogen complexes with different pincer backbone structures (see the Supporting Information).

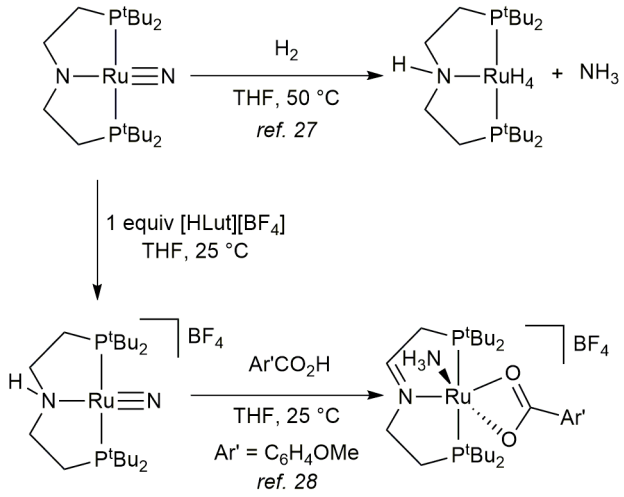

Scheme 2. Formation of ammonia from (PNP)Ru(N).

Based on these initial findings, we set out to independently synthesize a series of ruthenium hydrido dinitrogen complexes, with the goal of assessing how the distinct donor properties of the various pincer ligand states influence ruthenium-dinitrogen interactions. It is now well established that the transition metal oxidation state can greatly influence the extent of N_2 activation.[9,29–31] However, there have been far fewer systematic studies exploring how changes to the supporting ligand can influence N_2 activation. As shown in Scheme 3, ligand tuning has been accomplished by modification with Lewis or Brønsted acids or by reduction of the ligand.

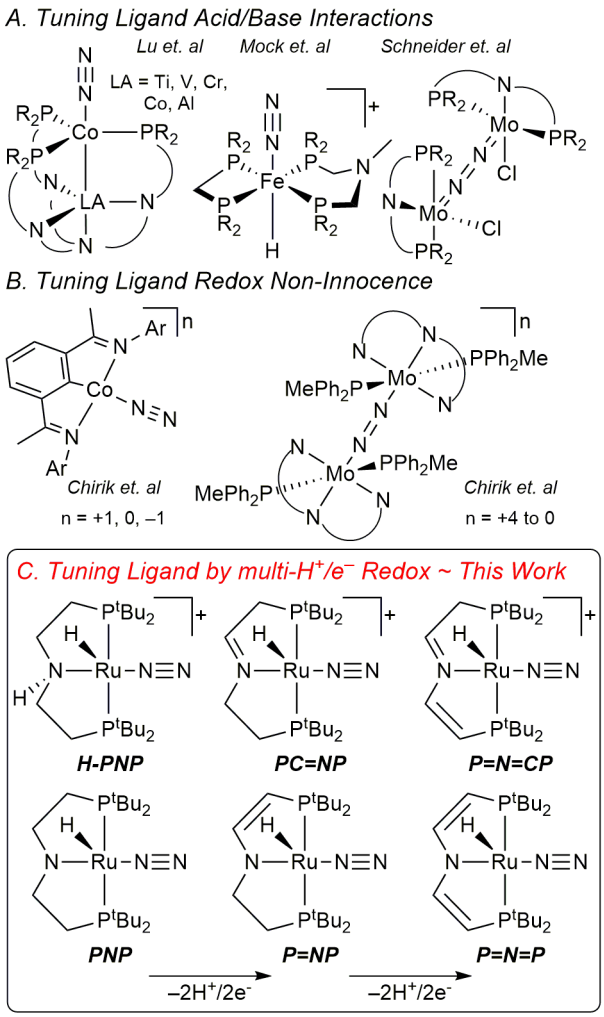

Scheme 3. Examples of tuning the bonding in N_2 ligands via acid/base interactions (A), redox non-innocence (B), and multi-proton, multi-electron redox (C) .

The impact of varying Lewis acids trans to the N_2 ligand was explored by Lu et al. using a $(MP_3)Co^{-1}(N_2)$ scaffold.[32] When a vanadium ion sits trans to N_2 ν_{NN} is 1971 cm^{-1}, whereas an aluminum ion trans to N_2 gives less activation (ν_{NN} = 1995 cm^{-1}).[32] Effects of ligand backbone protonation on N_2 activation have also been explored, with Mock et al. demonstrating a 25 cm^{-1} shift in ν_{NN} upon protonation of a pendent amine in $[(PN^{Me}P)(dmpm)Fe(H)(N_2)]^+$.[33] Similarly, dearomatization of the pyridine backbone of a rhodium N_2 complex resulted in a 31 cm^{-1} shift in

ν_{NN}.[34] Schneider et al. recently showed that protonation of the amide backbone in [(PNP)Mo(Cl)]$_2$(μ-N_2) leads to N–N bond cleavage and formation of [(H–PNP)Mo(N)(Cl)]$^+$.[35] Tuning via one-electron ligand reductions has been explored by Chirik et al., who found that varying the redox states of a bis(imino)pyridine ligand at Co leads to large shifts in ν_{NN} (2184 to 2046 cm^{-1} upon reduction by 2e$^-$).[36–38]

While the studies in Scheme 3A and 3B have focused on single proton or single electron changes, the ligand scaffold of Scheme 3C supports six different states covering a range of multiproton/multielectron changes (without involving ligand-centered radicals). Acid/base chemistry and net 2H$^+$/2e$^-$ transformations move between amine, amide, enamide, or imine ligand states.[39,40] Different ligand states have induced spin state changes in (diphosphinoamide)RuCl complexes upon 2H$^+$/2e$^-$ oxidation, indicating formal backbone oxidation has significant effects on the electronic structure.[40] These multiproton/multielectron formal oxidations are part of a broader trend of ligands featuring "chemical non-innocence".[28,41–45] Of particular note are Milstein's diphosphinopyridine ligands that adopt multiple backbone structures through dearomatization.[43] These ligands support Mo catalysts for NH_3 synthesis as well as Ru catalysts for hydrogen transfer and alcohol/amine coupling reactions.[18,46] The imine (PC=NP) and enamide (P=NP) backbone states of Scheme 3C are aliphatic analogues of the pyridine and dearomatized enamide states of Milstein's ligand.[43] Ir and Rh dinitrogen complexes supported by (P=N=P) have been reported,[47–49] but systematic studies exploring the influence of different (PNP) ligand states on N_2 activation are lacking.

Herein we report the synthesis of a family of *cis*-hydridodinitrogen ruthenium complexes of the formula (pincer)Ru(H)(N_2). All six ligand-based formal oxidation states are accessed in an

isostructural series for the first time, with pincer donor properties ranging from π-accepting and/or σ-donating L_3 systems to π- and σ-donating L_2X systems. The influence of the pincer ligand state on N_2 activation is assessed through crystallographic studies, IR spectroscopy, and ^{15}N NMR spectroscopy. The N_2 ligand in turn acts as a probe for the donor/acceptor properties of the different backbone states. The present system is noteworthy for providing a large number of isostructural complexes that each retain an N_2 ligand and a stable hydride (which could in principle be transferred to the pincer backbone, the N_2 ligand, or to a substrate in organometallic catalysis). The utility of these complexes will depend on the extent of N_2 activation afforded by the PNP ligand framework: strong activation would be amenable to N_2 fixation while weak activation would be ideal for organometallic catalysis in which labile N_2 ligands facilitate substrate binding.

Results & Discussion

Synthesis of neutral (pincer)Ru(H)(N_2) complexes

The Ru dichloride (H-PNP)Ru$(Cl)_2$ was prepared according to the previously reported procedure.[50] Treating a suspension of green (H-PNP)Ru$(Cl)_2$ in THF with 3 equiv KC_8 at –78 °C resulted in rapid formation of a dark red solution (Scheme 4). The isolated bright red powder was found to be diamagnetic, with a single resonance in the $^{31}P\{^1H\}$ NMR spectrum (δ 103.11) indicating a symmetric ligand backbone. ^1H NMR spectroscopy revealed the presence of a Ru hydride (δ –24.08), but no amine proton. The solid-state IR spectrum features a strong stretch at 2048 cm^{-1}, consistent with a terminally bound N_2 ligand; the spectrum in THF is essentially identical (ν_{NN} = 2050 cm^{-1}). The N_2 ligand was further characterized using natural abundance ^1H-^{15}N HMBC experiments. The hydride couples to the Ru-bound nitrogen of the N_2 ligand (Nα, δ

308.81), while the ethylene linker protons couple only to N_{PNP} (δ 143.19). The product is assigned as the new hydrido dinitrogen complex (PNP)Ru(H)(N_2) (**1**, Scheme 4).

Single crystals of **1** suitable for X-ray diffraction were grown by slow evaporation of a concentrated pentane solution. The structure (Figure 1, Table 1) confirms an end-on terminal N_2 ligand trans to the amide backbone. The Ru–N_{PNP} distance (2.008(3) Å) is similar to other (PNP)Ru complexes,[40,50] and the Ru–Nα distance (1.927(3) Å) is in the range of Ru(H)(N_2) complexes supported by other ligands.[18,20,21,29,51,52] The N_{PNP}–Ru–Nα angle of 167.38(14)° is somewhat distorted from the typical angles of square planar or square pyramidal (PNP)Ru complexes.[27,39,40,50] The N–N distance (1.118(5) Å) and N_2 stretching frequency (ν_{NN} = 2050 cm^{-1} in THF) indicate that the N_2 ligand in **1** is weakly activated.[8]

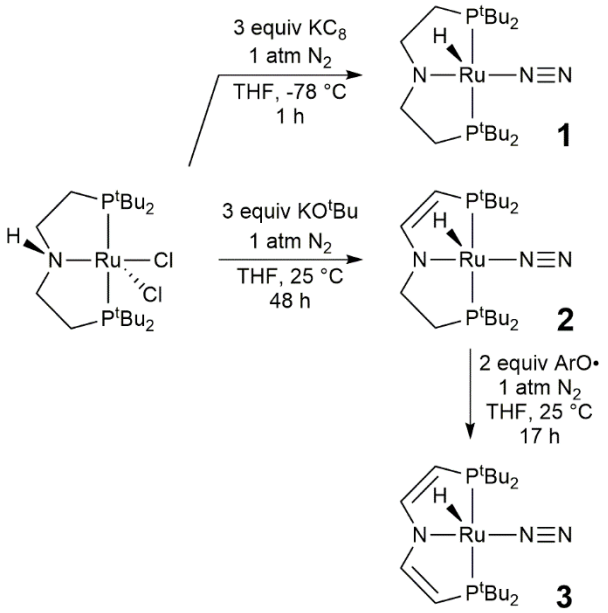

Scheme 4. Synthesis of complexes **1-3**.

The enamide ligand state, featuring formal $2H^+/2e^-$ oxidation of the ligand backbone, was targeted next. Utilizing an approach that had proven successful for a trimethylphosphine Ru

complex,[53] a green suspension of (H-PNP)Ru(Cl)$_2$ in THF was treated with 3 equiv KO^{t}Bu. An intensely purple colored solution quickly formed, from which a purple solid was isolated in 89% yield (Scheme 4). Initial evidence for an asymmetric ligand backbone structure is found in the ^{31}P{^{1}H} NMR spectrum, which features two doublets (δ 97.34, J = 252.8 Hz; δ 82.31, J = 249.8 Hz). ^{1}H NMR spectroscopy reveals the signatures expected of the enamide backbone, including a doublet of doublets for the N–C*H*=CH–P resonance (δ 7.23), and four inequivalent ^{t}Bu doublets. A surprisingly upfield chemical shift is observed for the N–CH=C*H*–P proton in **2** (δ 3.69), suggesting some contribution from an imine resonance contribution that places a negative charge on the ligand backbone.[53] A hydride resonance (δ –29.17) exhibited a correlation with Nα (δ 309.22) in a ^{1}H-^{15}N HMBC NMR experiment. IR spectroscopy in THF (ν_{NN} = 2057 cm^{-1}) confirms a bound N_2 ligand, leading to the assignment as (P=NP)Ru(H)(N_2) (**2**, Scheme 4). Crystals of **2** were grown from slow evaporation of a concentrated pentane solution and X-ray diffraction confirmed the expected structure with a single vinyl linker (C=C 1.368(6) Å) in the backbone. Complex **2** (Figure 1, Table 1) features a Ru–N_{PNP} distance of 2.036(3) Å, a Ru–Nα distance of 1.921(3) Å, and a N–N distance of 1.102(4) Å.

The dienamide (P=N=P) backbone was accessible by direct oxidation of the ligand via hydrogen atom abstraction (HAA) by 2,4,6-tri-*tert*-butylphenoxyl radical (ArO$^\bullet$). Guided by a related protocol for oxidation of (PNP)Co complexes,[39] treatment of **2** with 2 equiv ArO$^\bullet$ led to a color change from purple to maroon and isolation of a new product in 96% yield. The ^{31}P{^{1}H} NMR spectrum shows a single resonance (δ 85.87) suggesting a symmetric backbone. The ^{1}H NMR spectrum features a characteristic downfield resonance (δ 7.35) and a hydride resonance at –29.84 ppm. The N_2 ligand is apparent in the IR spectrum in THF (2072 cm^{-1}) and in NMR studies

(Nα δ 307.30), allowing assignment as (P=N=P)Ru(H)(N_2) (**3**, Scheme 4) and completing the anionic PNP series. Slow evaporation of a concentrated pentane solution of **3** afforded red single crystals. X-ray analysis (Figure 1, Table 1) confirmed the presence of a planar P=N=P ligand backbone (C=C 1.344(7), 1.354(7) Å; Ru–N_{PNP} 2.053(4) Å) and retention of the N_2 ligand (N–N 1.095(5) Å, Ru–Nα 1.929(4) Å).

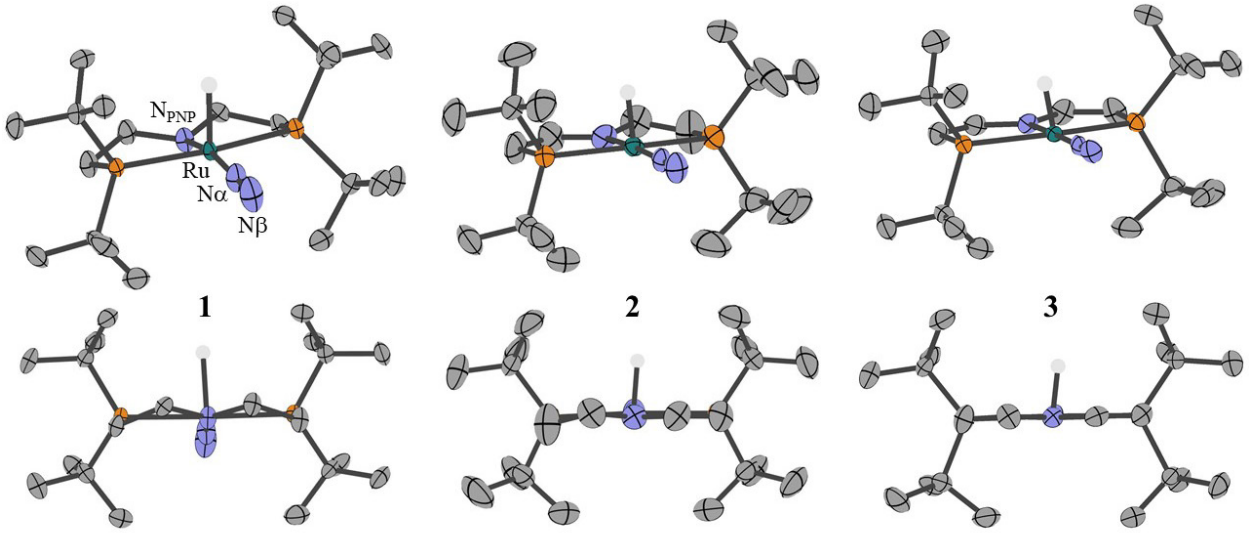

Figure 1. Structural representations of complexes **1**, **2**, and **3** from XRD studies, with ellipsoids at 50% probability level. See Table 1 for metrical parameters and the SI for full details.

Table 1. Crystallographic, NMR and IR data for complexes **1**–**3**.

	(PNP)Ru(H)(N_2) **(1)**	(P=NP)Ru(H)(N_2) **(2)**	(P=N=P)Ru(H)(N_2) **(3)**
Ru–N_{PNP} (Å)	2.008(3)	2.036(3)	2.053(4)
Ru–Nα (Å)	1.927(3)	1.921(3)	1.929(4)
Nα–Nβ (Å)	1.118(5)	1.102(4)	1.095(5)
N_{PNP}–Ru–Nα(°)	167.38(14)	176.74(12)	178.54(16)
^{1}H Ru–H (ppm in d_8-THF)	–24.08	–29.17	–29.84
^{15}N N_{PNP} (ppm in d_8-THF)	143.19	131.77	161.63
^{15}N Nα (ppm in d_8-THF)	308.81	309.22	307.30

ν_{NN} (cm^{-1} in THF)	2050	2057	2072

An alternative synthetic strategy to reach hydrido dinitrogen complexes was envisioned based on initial oxidation of the ligand backbone of the ruthenium chloride precursor followed by installation of the hydride.[39,40,50,53] Schneider and co-workers previously developed routes from (H-PNP)Ru(Cl)$_2$ to monochloride complexes with dialkylamide- and dienamide-based pincer ligands.[40,50] Stirring (PNP)Ru(Cl) with CoCp*$_2$ in THF for two weeks provided hydride complex **1** in around 50% yield (Scheme 5). No deuterium incorporation into the product was observed when the reaction was carried out in deuterated solvent (THF-d_8), suggesting that the hydride ligand is formed by hydrogen atom transfer from decamethylcobaltocene.[50] Similarly, complex **3** was observed spectroscopically upon treating the dienamide backbone complex (P=N=P)Ru(Cl) with 1 equiv of CoCp*$_2$ in THF. If benzene-d_6 is used as the solvent, the protio hydride is still formed, again suggesting that CoCp*$_2$ may be the hydrogen donor.

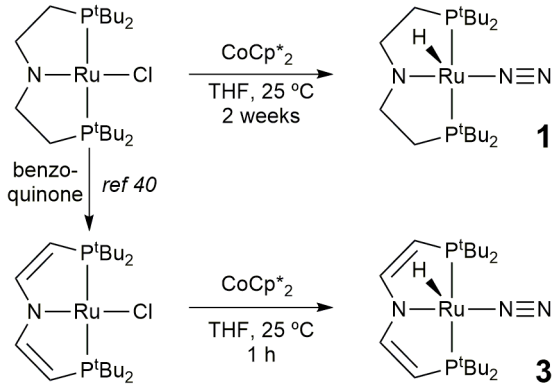

Scheme 5. Alternative synthetic routes to complexes **1** and **3**.

Once formed, the ruthenium hydrides are also quite robust. Complex **3** was found to be stable in the presence of excess ArO$^{\bullet}$ at elevated temperatures (60 °C), even though hydrogen atom abstraction might be anticipated. The strong base KO^{t}Bu could be used in the synthesis of complex

2 and the purification of complex **3** because the hydrides were not acidic enough to be deprotonated.

Synthesis of cationic [(pincer)Ru(H)(N_2)][BF_4] complexes

Treatment of **1** with 0.95 equiv 2,6-lutidinium tetrafluoroborate ([HLut][BF_4]) in THF resulted in a color change from red to dark orange, providing an orange-brown powder in 86% yield upon workup (Scheme 6). The ^{1}H NMR spectrum contains a Ru–H signal (δ –30.43) and a N–*H* resonance (δ 4.54) indicating protonation at the PNP ligand backbone nitrogen (the symmetric saturated ethylene linkers are retained). A singlet in the $^{31}P\{^1H\}$ NMR spectrum (δ 86.97) further confirms a symmetric backbone. A correlation between the hydride resonance and the Nα resonance of the N_2 ligand was observed at 299.90 ppm. IR spectroscopy indicates retention of N_2 (ν_{NN} = 2109 cm^{-1}, THF), consistent with formation of [(H-PNP)Ru(H)(N_2)][BF_4] (**4**, Scheme 6). The ν_{NN} value is indicative of a very weakly activated N_2.

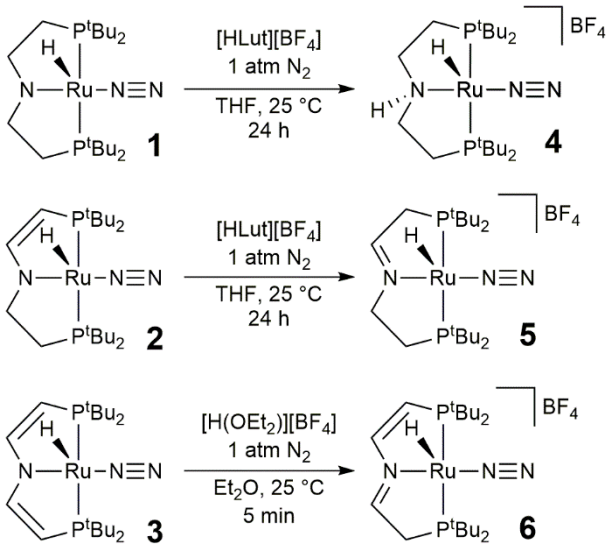

Scheme 6. Synthesis of complexes **4-6**.

Single crystals were grown by vapor diffusion of pentane into a concentrated acetone solution of **4**. An X-ray diffraction study confirms that **4** adopts the expected square pyramidal geometry with a *cis*-hydridodinitrogen configuration (Figure 2, Table 2). Protonation of the backbone amine occurs trans relative to the hydride and results in a long Ru–N_{PNP} distance (2.116(5) Å). A hydrogen bonding interaction is observed between the BF_4 counterion and the amine proton (*H*--F distance 2.101 Å, N--F distance 3.034(6) Å). Complex **4** features a short N–N bond (1.083(8) Å), further consistent with limited N_2 activation.

Treatment of **2** with 0.95 equiv [HLut][BF_4] in THF results in a color change from purple to orange, with subsequent isolation affording a bright orange powder in 95% yield (Scheme 6). Two doublets observed by $^{31}P\{^1H\}$ NMR spectroscopy (δ 92.45, J = 240.2 Hz; δ 89.51, J = 239.9 Hz) indicate the presence of an asymmetric ligand backbone. The ^1H NMR spectrum features a downfield resonance (δ 8.51, J = 24.3 Hz) characteristic of an imine ligand (PC=NP). The upfield hydride resonance (δ –29.23) correlates with a bound N_2 ligand, also located relatively upfield (Nα δ 294.69). The orange powder is thus assigned as [(PC=NP)Ru(H)(N_2)][BF_4] (**5**, Scheme 6). The strong IR stretch in **5** (ν_{NN} = 2117 cm^{-1}, THF) indicates weak activation of N_2. Vapor diffusion of pentane into a concentrated acetone solution of **5** afforded red-orange crystals suitable for X-ray analysis (Figure 2, Table 2). A short N–C bond (1.315(6) Å) in the backbone of **5** is consistent with an imine ligand backbone (Ru–N_{PNP} bond 2.0638(18) Å). The N_2 ligand is retained cis to the hydride (Ru–Nα 1.9275(19) Å, N–N 1.102(3) Å).

Protonation of **3** with 0.95 equiv [H(OEt_2)][BF_4] in Et_2O results in an immediate precipitation of an orange solid isolated in 85% yield (Scheme 6). ^1H NMR spectroscopy shows retention of the hydride at –28.94 ppm, as well as several downfield resonances (δ 8.75, δ 7.67, δ

6.46) indicative of multiple sp^2 carbons in the ligand backbone. Unlike complexes **2** and **3**, in complex **6** the NCHC*H*P proton is in the range expected for a vinyl linker (δ 6.46). Two doublet resonances in the ^{31}P NMR spectrum (δ 91.40, J = 240.4 Hz; δ 84.82, J = 239.8 Hz) provide further evidence for a vinyl imine backbone (P=N=CP) arising from selective protonation at the ligand backbone (no reaction with Ru–H is evident). The N_2 ligand is retained (ν_{NN} = 2123 cm^{-1}, THF), allowing assignment as $[(P{=}N{=}CP)Ru(H)(N_2)][BF_4]$ (**6**, Scheme 6). Layering a concentrated acetone solution of **6** with pentane at room temperature led to the formation of yellow needles suitable for X-ray analysis. Complex **6** (Figure 2, Table 2) features the expected planar backbone and *cis*-hydridodinitrogen geometry, with a Ru–N_{PNP} bond length of 2.070(4) Å, a Ru–Nα distance of 1.936(4) Å, and a N–N distance of 1.101(5) Å.

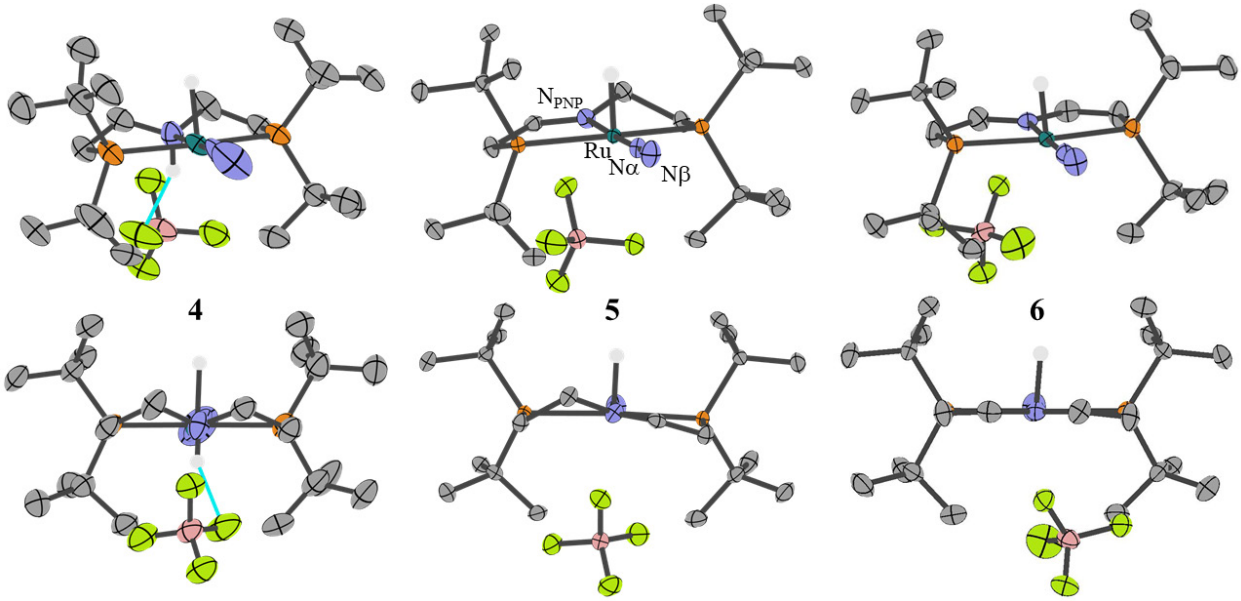

Figure 2. Structural representations of complexes **4**, **5**, and **6** from XRD studies, with ellipsoids at 50% probability level. Crystals of **5** featured backbone atoms disordered over two positions (major site shown, see SI for details). See Table 2 for metrical parameters and the SI for full details.

Table 2. Crystallographic, NMR and IR data for complexes **4**–**6**.

	$[(H\text{-}PNP)Ru(H)(N_2)]^+$ **(4)**	$[(PC{=}NP)Ru(H)(N_2)]^+$ **(5)**	$[(P{=}N{=}CP)Ru(H)(N_2)]^+$ **(6)**
$Ru–N_{PNP}$ (Å)	2.116(5)	2.0638(18)	2.070(4)
Ru–Nα (Å)	1.945(6)	1.9275(19)	1.936(4)
Nα–Nβ (Å)	1.083(8)	1.102(3)	1.101(5)
N_{PNP}–Ru–Nα(°)	178.44(19)	176.94(8)	178.54(15)
^{1}H Ru–H (ppm in CD_2Cl_2)	–30.43	–29.23	–28.94
^{15}N N_{PNP} (ppm in CD_2Cl_2)	36.61	272.03	274.42
^{15}N Nα (ppm in CD_2Cl_2)	299.90	294.69	295.53
ν_{NN} (cm^{-1} in THF)	2109	2117	2123

Structural and Spectroscopic Trends Related to N_2 Activation.

The isostructural series of neutral and cationic N_2 complexes enables comparisons of the donor properties of the six different ligand states. The extent of N_2 activation can be probed using crystallography (based on the N–N distance) or IR spectroscopy (ν_{NN}). The crystallographic data of complexes **1**-**6** provide insight into the bonding of the pincer ligand and the N_2 ligand. Changes in the nitrogen donor properties are reflected in the bond distances between the metal and the central donor of the pincer ($Ru–N_{PNP}$). The $Ru–N_{PNP}$ distance increases steadily moving from the saturated dialkylamide backbone of **1** (2.008(3) Å) to the enamide backbone of **2** (2.036(3) Å) to the dienamide backbone of **3** (2.053(4) Å). This trend is in accord with the PNP ligand being a stronger π-donor than the P=NP and P=N=P ligands. The presence of an amine (H-PNP) in the backbone of complex **4** is clearly reflected in the long $Ru–N_{PNP}$ distance of 2.116(5) Å. Complexes **5** and **6** feature an imine backbone and have similar $Ru–N_{PNP}$ distances (~2.07 Å) that are between the neutral complexes **1**-**3** and cationic complex **4**. The observed distances are consistent with the imine of **5** and **6** interacting in a σ-donating and π-backbonding fashion. The geometry of the

backbone is also reflective of changes in formal oxidation state. The backbone flattens significantly as unsaturation is introduced to the pincer ligand moving from **1** to **2** to **3** (Figure 1). A similar trend is observed for **4**, **5**, and **6** (Figure 2).

The N–N distance in five of the six complexes is within error of free N_2. All six complexes are clearly in the weak activation regime, with no evidence for any formal reduction in bond order. Within this regime, however, no clear trends are observed; this is probably due to crystallographic uncertainty associated with terminal diatomic ligands coupled with small perturbations in N–N distance.[54] Complex **1** has a slightly elongated N–N bond (1.118(5) Å), as well as several other structural parameters that are distinct from complexes **2**-**5**. For example, complex **1** alone features a bent N_{PNP}–Ru–Nα angle (167.38(14)°), which may explain the distinct downfield hydride shift (δ –24.08) observed by ^{1}H NMR spectroscopy.

Although no trend in the N–N distances is observed crystallographically, the IR stretching frequency of the N–N bond correlates nicely with changes in the ligand backbone. For the neutral complexes supported by anionic L_2X-type donors, ν_{NN} increases alongside the lengthening Ru–N_{PNP} bond upon sequential $2H^+/2e^-$ oxidation of the backbone from **1** (PNP) to **2** (P=NP) to **3** (P=N=P). The addition of π conjugation in **2** and **3** shifts electron density away from the amide nitrogen, making the PNP ligand a weaker π donor and thus decreasing the π-backdonation that promotes N_2 activation (ν_{NN} shifts by 22 cm^{-1} in THF). The change in hybridization of the backbone linkers may also have a minor influence on the σ-donor properties. The related carbonyl complexes (L)Ru(Cl)(CO) (L = PNP, P=NP, P=N=P) also showed decreased CO backbonding upon increased unsaturation of the pincer backbone.[40] The N_2 ligand in complex **1** is the most

activated, on the basis of the lowest energy ν_{NN} value and the longest N–N bond length, all in accord with the pincer ligand in this complex having the strongest π donor ability.

The cationic complexes all have significantly higher ν_{NN} values, indicating weaker backbonding and less activated N_2 ligands. The N_2 ligand becomes less activated upon oxidation of the H-PNP ligand backbone of **4** (ν_{NN} = 2109 cm^{-1}, THF) to an imine backbone in **5** (PC=NP, ν_{NN} = 2117 cm^{-1}, THF) and a vinyl imine backbone in **6** (P=N=CP, ν_{NN} = 2123 cm^{-1}, THF). This trend may be due to the imine backbones in **5** and **6** acting as π-acceptors, whereas the secondary amine in the H-PNP pincer ligand of complex **4** is a pure σ-donor. The incorporation of competing imine π-acceptors results in reduced π-backdonation from Ru into the N_2 ligand.

The N_2 ligand was further characterized by the ^{15}N chemical shift obtained through ^{1}H-^{15}N HMBC experiments. Attempts to correlate ^{15}N chemical shifts with measures of N_2 activation have been limited,[6] but the *cis*-hydridodinitrogen structures of **1**-**6** enable indirect detection through a short coupling pathway ($^{2}J_{NH}$). Interestingly, the ^{15}N chemical shifts of **1**-**6** were not highly sensitive to changes in the pincer backbone. The overall charge of the complex led to the most significant change in chemical shift, with ^{15}N resonances for neutral complexes **1**-**3** near 309 ppm and resonances for the cationic complexes **4**-**6** appearing near 295 ppm. The upfield shift is consistent with a decrease in population of the N_2 π* orbitals due to stabilization of the Ru d-orbitals in the cationic complexes, thereby modulating the paramagnetic shielding term.[55,56]

Displacement of the N_2 Ligand

Retention of weak N_2 binding across all ligand backbone states suggests that N_2 displacement should be facile, regardless of the ligand backbone structure. We thus sought to probe

the substitutional lability of the N_2 ligand. When a solution of **1** in C_6D_6 in a Teflon-sealed NMR tube was placed under 1 atm CO and inverted, the color immediately changed from red to yellow. After the excess CO was removed by three freeze-pump-thaw cycles, $^{31}P\{^1H\}$ NMR spectroscopy revealed a prominent singlet at 111 ppm assigned to (PNP)Ru(H)(CO) (**1a**) (75% yield by NMR) (Scheme 7). The carbonyl complex **1a** has been used for alcohol oxidation and nitrile hydrogenation.[57,58]

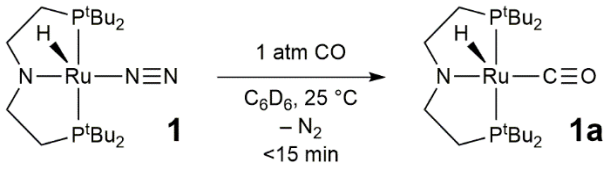

Scheme 7. Displacement of the N_2 ligand with CO.

The reaction of cationic N_2 complexes with an anionic donor was next explored. The reaction of **5** with 1.1 equiv sodium 4-methoxybenzoate ([Na][O_2CAr']) yielded a yellow-orange powder in 97% yield. ^{31}P NMR spectroscopy contained two doublets (δ 91.51, J = 314.5 Hz; δ 86.00, J = 314.4 Hz) showing that the unsaturated backbone is retained. The new species features a downfield hydride resonance (δ –22.17) representing a 5 ppm shift relative to the starting material **5**, which could be due to the binding of a ligand trans to the hydride. IR spectroscopy shows no strong features between 2200 and 1900 cm^{-1}, indicating that the N_2 ligand was displaced. The structure is thus assigned as a κ^2-benzoate adduct, (PC=NP)Ru(H)(κ^2-O_2CAr') (**7**, Scheme 8).

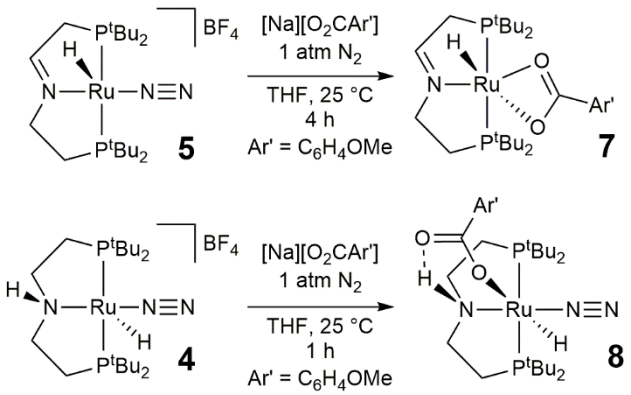

Scheme 8. Reactions of N_2 complexes with a benzoate derivative.

Analogous treatment of **4** with 1.1 equiv [Na][O_2CAr'] in THF resulted in a color change from orange to yellow, leading to isolation of a pale-yellow solid in 74% yield. ^{1}H NMR spectroscopy confirms retention of the H-PNP ligand backbone, including the amine proton (δ 10.68). The downfield chemical shift of the hydride (δ –18.83) suggests the presence of a trans donor ligand. In surprising contrast to the preceding reaction, IR spectroscopy revealed that the N_2 ligand is retained and activated (ν_{NN} 2095 cm^{-1} in THF, c.f. ν_{NN} 2109 cm^{-1} in **4**). On the basis of these spectroscopic features, the produced species can be assigned as (H-PNP)Ru(H)(κ^1-O_2CAr')(N_2) (**8**, Scheme 8). Colorless needles of **8** suitable for x-ray diffraction could be grown via slow evaporation of a concentrated diethyl ether solution (Figure 3). The structure confirmed a hydrogen bonding interaction between the carbonyl and pincer amine proton (N–*H*--O distance 1.811 Å, N--O distance 2.709(5) Å). Similar carboxylate interactions have been invoked as intermediates in CO_2 reduction and both methanol and formic acid dehydrogenation.[59–62]

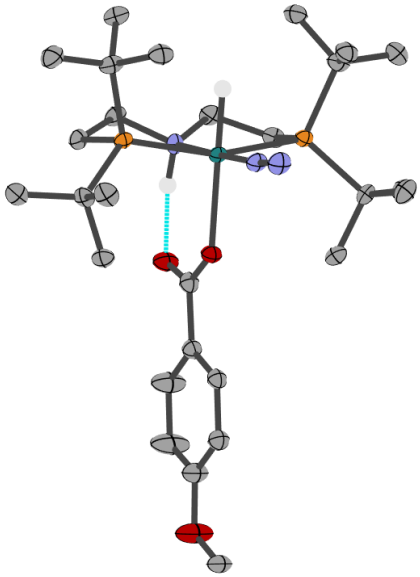

Figure 3. Molecular structure of (H-PNP)Ru(H)(κ^1-O_2CAr')(N_2) (**8**). Ellipsoids are drawn at the 50% probability level with select hydrogen atoms shown. Selected distances (Å) and angles (deg): Ru–N_{PNP} 2.136(4), Ru–Nα 1.912(4), Nα–Nβ 1.114(6), N_{PNP}–Ru–Nα 178.72(16).

Divergent reactivity upon benzoate addition to complexes **4** and **5** may be due to the difference in backbone states. Benzoate displaces the N_2 ligand in complex **5** to produce κ^2-benzoate adduct **7**. In contrast, benzoate binds to complex **4** without displacement of N_2. We hypothesize that retention of N_2 is due to the hydrogen bonding interaction between the benzoate carbonyl oxygen and the amine proton on the H-PNP backbone (Figure 3). The hydrogen bond enforces benzoate binding in a κ^1 fashion trans to the hydride, preventing any disruption of the N_2 binding site trans to the pincer ligand backbone.

Conclusions

A family of ruthenium *cis*-hydridodinitrogen complexes with conserved structural features across six multiproton/multielectron ligand oxidation states was examined. These six complexes

are noteworthy for retaining the *cis*-hydridodinitrogen motif, providing the first example of an isostructural series supported by each of the six possible analogues of PNP.

The isostructural series provides an opportunity to compare the ligand donor properties of the various pincer ligand backbones. The fully saturated, L_2X-type PNP ligand state is the strongest π-donor, with the furthest degree of N_2 activation (N–N bond 1.119(5) Å, $\nu_{NN} = 2048\ cm^{-1}$). Ligand oxidation to enamide (P=NP) and dienamide (P=N=P) results in less N_2 activation, with stepwise shifts of ν_{NN} to higher energy. Across this series, the PNP ligand is the strongest π-donor, followed by the enamide and then dienamide ligands. This trend is nicely aligned with the related series of Ru carbonyl complexes previously reported by Schneider and co-workers.[40]

Protonation of the PNP ligand shuts down π interactions, and H-PNP is the lone example of a σ-only donor in this series. This removal of π donation correlates with the N_2 ligand becoming less activated. The enamide ligands P=NP and P=N=P can also be protonated, with the protonation occurring at a carbon on the backbone. The resulting imine-based ligands PC=NP and P=N=CP are possible π-acceptors, based on a further shift towards more weakly activated N_2 ligands.

The presence of a stable Ru–H fragment in each complex suggests that hydrides are thermodynamically favored relative to transfer to N_2 (to form RuNNH species) or the ligand backbone. With no evidence of N_2 reactivity and structural and spectroscopic studies establishing weakly activated N_2 ligands in all cases, the present complexes do not appear to be promising for ammonia synthesis. On the other hand, the presence of a weakly activated N_2 ligand present in each complex could be ideal for applications in organometallic catalysis.

Facile N_2 substitution was observed upon treatment with CO, but benzoate binding is more subtle: when benzoate binds to cationic $[(H\text{-}PNP)Ru(H)(N_2)]^+$, the N_2 ligand is retained, whereas N_2 release is observed upon benzoate addition to $[(PC{=}NP)Ru(H)(N_2)]^+$. This divergent reactivity is attributed to a secondary coordination sphere interaction of the H-PNP ligand state, where a hydrogen bond between the amine proton and benzoate oxygen leads to a κ^1 binding mode and retention of N_2.

Acknowledgements

Q.J.B., B.M.L., and A.J.M.M. gratefully acknowledge initial support from the National Science Foundation (NSF) Center for Enabling New Technologies through Catalysis (CENTC), CHE-1205189 and continuing support from the NSF Chemical Catalysis program under Grant No. CHE-1665135. Q.J.B. acknowledges support from the University of North Carolina at Chapel Hill (Morrison Research Fellowship) and NSF Graduate Research Fellowship Program (DGE-1650116). A.J.M.M. is an Alfred P. Sloan Fellow. The authors thank B. Ehrmann for assistance with mass spectrometry, P. White and D. Dickie for assistance with X-ray crystallography, and K. Krogh-Jespersen for helpful discussions. S.S. thanks the European Research Council (ERC Grant Agreement 646747) for financial support.

Experimental Section

General Considerations. All manipulations were carried out under an N_2 atmosphere using standard glovebox and Schlenk techniques. Under standard glovebox operating conditions, pentane, diethyl ether (Et_2O), benzene, toluene, dichloromethane (CH_2Cl_2), and tetrahydrofuran (THF) were used without purging, such that traces of those solvents were present in the atmosphere and in the solvent bottles. ^1H, $^{31}P\{^1H\}$, $^{19}F\{^1H\}$, $^{13}C\{^1H\}$, and ^1H-^{15}N HMBC spectra were recorded

on 400 or 600 MHz spectrometers at 298 K. NMR solvents were purchased from Cambridge Isotopes Laboratories, Inc. Benzene-d_6 (C_6D_6) was freeze–pump–thaw degassed three times before drying by passage through a small column of activated alumina and stored over 3 Å molecular sieves. Tetrahydrofuran-d_8 (THF-d_8) and dichloromethane-d_2 (CD_2Cl_2) were freeze–pump–thaw degassed three times before drying by passage over two small columns of activated alumina and stored over 3 Å molecular sieves. ^{1}H and ^{13}C chemical shifts are reported relative to residual protio solvent resonances.[63] ^{31}P chemical shifts are reported relative to an 85% H_3PO_4 external standard (δ 0). ^{19}F chemical shifts are reported relative to an 10% w/v CCl_3F in $CDCl_3$ external standard (δ 0). ^{15}N chemical shifts are reported relative to neat nitromethane external standard (δ 376.86). (H-PNP)$RuCl_2$,[50] (PNP)$RuCl$,[50] KC_8,[64] 2,4,6-tri-*tert*-butylphenoxyl radical (ArO•),[65] and 2,6-lutidinium tetrafluoroborate ([HLut][BF_4])[66] were prepared following literature procedures. Sodium 4-methoxy benzoate ([Na][O_2CAr']) was prepared by stirring an excess of 4-methoxybenzoic acid with sodium hydride in THF and collecting the resulting insoluble white powder and drying under vacuum. KO^{t}Bu was purchased from Sigma Aldrich and purified via sublimation. All other reagents were commercially available and used without further purification. High-resolution mass spectrometry (HRMS) was carried out with an LTQ FT (ICR 7T) (ThermoFisher, Bremen, Germany) mass spectrometer. Samples (in toluene, dichloromethane, or acetone solution) were introduced via a microelectrospray source at a flow rate of 3 μL/min. Xcalibur (ThermoFisher, Bremen, Germany) was used to analyze the data. Molecular formula assignments were determined with Molecular Formula Calculator (v 1.2.3). Infrared spectroscopy was carried out with a Thermo Scientific Nicolet iS5 FT-IR equipped with Quest single reflection ATR accessory for solid-state measurements or equipped with a iD1 Transmission Accessory (Thermo Scientific) for solution measurements in a demountable liquid cell with CaF_2 windows (0.05 mm pathlength) (Pike

Technologies Inc.). Single-crystal X-ray diffraction data was collected on a Bruker APEX-II CCD diffractometer at 100 K with Cu Kα radiation (λ = 1.54175 Å). Using Olex2,[67] the structures were solved with the XT intrinsic phasing program[68] and refined with the XL refinement program[69] using least squares minimization. See the SI for additional crystallographic details for each complex. Elemental analysis was performed at Robertson Microlit Laboratories (Ledgewood, NJ); the dinitrogen complexes invariably exhibited low nitrogen content.

Synthesis of (PNP)Ru(H)(N_2) (1). In a glovebox, (H-PNP)Ru($Cl)_2$ (23.5 mg, 0.044 mmol) was suspended in 5 mL THF and KC_8 (17.8 mg, 0.132 mmol) was suspended in 4 mL THF and both solutions were cooled to –78 °C. After 10 min, the suspensions were combined, resulting in the rapid formation of a dark red solution that was kept at –78 °C for 1 h with periodic agitation to ensure sufficient mixing. The resulting solution was filtered and dried *in vacuo*. The resulting dark red solid was extracted with benzene (3 x 2mL) and filtered to give a dark red solution that was lyophilized to yield a bright red powder (20.8 mg, 96.5% yield). The material was 92.2% pure, with 4.5% impurity of **2** and 3.5% impurity of (PNP)Ru($H)_3$[27] as determined by multinuclear NMR spectroscopy. NMR and IR spectroscopy and mass spectrometry are reported for the isolated powder. X-ray quality crystals were grown by slow evaporation of a concentrated pentane solution at 25 °C. Elemental analysis was performed on recrystallized material. **^{1}H NMR** (600 MHz, C_6D_6): δ 3.30 (m, 2H, NCH_2), 2.87 (m, 2H, NCH_2), 1.78 (m, 4H, PCH_2), 1.29 (m, 36H, C(C$H_3)_3$), –23.80 (t, 17.0 Hz, 1H, Ru*H*). **^{13}C{^{1}H} NMR** (151 MHz, C_6D_6) δ 63.77 (t, 6.9 Hz, N*C*H_2), 35.76 (t, 7.0 Hz, *C*($CH_3)_3$), 35.51 (t, 7.9 Hz, *C*($CH_3)_3$), 29.74 (t, 2.8 Hz, C(*C*$H_3)_3$), 28.22 (t, 3.1 Hz, C(*C*$H_3)_3$), 24.98 (t, 6.9 Hz, P*C*H_2). **^{31}P{^{1}H} NMR** (243 MHz, C_6D_6) δ 102.55 (s). **^{1}H-^{15}N HMBC NMR** (C_6D_6): δ 309.43 (Nα), 146.93 (N_{PNP}). **^{1}H NMR** (600 MHz, THF): δ 3.15 (m, 2H, NCH_2), 2.77 (m, 2H, NCH_2), 2.13 (m, 2H, PCH_2), 1.85 (m, 2H, PCH_2), 1.38 (m, 36H, C(C$H_3)_3$), –24.08 (t, 17.0 Hz,

1H, Ru*H*). **^{31}P{^{1}H} NMR** (162 MHz, THF) δ 103.11 (s). **^{1}H-^{15}N HMBC NMR** (THF): δ 308.81 (Nα), 143.19 (N_{PNP}). **IR** (solid, cm^{-1}) ν(N_2) 2048 cm^{-1}. **IR** (solution, THF, cm^{-1}) ν_{NN} 2050 cm^{-1}. **HRMS** (ESI^+) *m/z* [(PNP)Ru(H)(N_2) +H^+]$^+$ calcd for $C_{20}H_{46}N_3P_2Ru$, 492.22065; found 492.22104. *Alternative synthesis:* A mixture of (PNP)RuCl (50 mg, 0.100 mmol) and $CoCp_2^*$ (39.9 mg, 0.121 mmol) was dissolved in cold THF (–35 °C). After two weeks at –35 °C, a yellow precipitate had formed. The solid was filtered off, extracted with THF (2 x 5 mL) and then all solutions were combined and dried *in vacuo*. The resulting greenish solid was extracted with pentanes (3 x 5 mL) and filtered. Recrystallization from pentane at –35 °C afforded red crystals (27.6 mg, 56.0% yield). **Anal. Calcd** for $C_{20}H_{45}N_3P_2Ru$: C, 48.96; H, 9.25; N, 8.56. Found: C, 49.23; H, 8.85; N, 7.30.

Synthesis of (P=NP)Ru(H)(N_2) (2). In a glovebox, solid KO^{t}Bu (24.9 mg; 0.222 mmol) was added to a suspension of (H-PNP)Ru($Cl)_2$ (39.5 mg; 0.074 mmol) in 10 mL THF. The resulting dark purple solution was stirred for 48 h before solvent was removed under vacuum. The resulting solids were extracted with pentane (2 × 3 mL), filtered, and dried under vacuum yielding a purple solid. The purple solid was taken up in 2 mL of benzene and lyophilized to yield a purple powder (32.0 mg, 89 % yield, 98.0% pure by multinuclear NMR spectroscopy). NMR and IR spectroscopy and mass spectrometry are reported for the isolated powder. X-ray quality crystals were grown by slow evaporation of a concentrated pentane solution at 25 °C. Elemental analysis was performed on recrystallized material. **^{1}H NMR** (600 MHz, C_6D_6): δ 7.49 (dd, 42.8 Hz, 5.4 Hz, 1H, NC*H*), 3.94 (m, 1H, PC*H*), 3.35 (m, 1H, NCH_2), 3.13 (m, 1H, NCH_2), 1.50 (m, 1H, PCH_2), 1.46 (d, 13.1 Hz, 9H, C(CH_3)$_3$), 1.41-1.35 (m, 1H, PCH_2) 1.38 (d, 12.4 Hz, 9H, C(CH_3)$_3$), 1.15 (d, 12.5 Hz, 9H, C(CH_3)$_3$), 1.10 (d, 12.3 Hz, 9H, C(CH_3)$_3$), –28.81 (t, 17.1 Hz, 1H, Ru*H*). **^{13}C{^{1}H} NMR** (151 MHz, C_6D_6) δ 168.62 (dd, 22.1, 3.2 Hz, N*C*H), 75.23 (d, 38.7 Hz, P*C*H), 59.24 (dd, 7.7 Hz, 1.7 Hz, NCH_2), 38.83 (d, 16.7 Hz, *C*(CH_3)$_3$), 36.05 (dd, 11.3, 2.1 Hz, *C*(CH_3)$_3$), 35.18 (dd, 1z5.5 Hz, 2.55

Hz, $C(CH_3)_3$), 34.39 (dd, 18.2 Hz, 2.74 Hz, $C(CH_3)_3$), 29.49 (m, $C(CH_3)_3$), 28.74 (d, 5.2 Hz, $C(CH_3)_3$), 25.12 (d, 15.7 Hz, PCH_2). **$^{31}P\{^1H\}$ NMR** (243 MHz, C_6D_6) δ 96.85 (d, 253.4 Hz), 82.35 (d, 253.2 Hz). **^1H-^{15}N HMBC NMR** (C_6D_6): δ 311.47 (Nα), 139.81 (N_{PNP}). **^1H NMR** (600 MHz, THF): δ 7.23 (dd, 43.0 Hz, 5.4 Hz, 1H, NC*H*), 3.69 (m, 1H, PC*H*), 3.51 (m, 1H, NCH_2), 3.17 (m, 1H, NCH_2), 2.06 (m, 1H, PCH_2), 1.81 (m, 1H, PCH_2), 1.36 (d, 7.5 Hz, 9H, $C(CH_3)_3$), 1.34 (d, 7.6 Hz, 9H, $C(CH_3)_3$), 1.33 (d, 5.2 Hz, 9H, $C(CH_3)_3$), 1.31 (d, 5.0 Hz, 9H, $C(CH_3)_3$), –29.17 (t, 17.2 Hz, 1H, Ru*H*).). **$^{31}P\{^1H\}$ NMR** (162 MHz, THF) δ 97.34 (d, 252.8 Hz), 82.31 (d, 249.8 Hz). **^1H-^{15}N HMBC NMR** (THF): δ 309.22 (Nα), 131.77 (N_{PNP}). **IR** (solid, cm^{-1}) ν_{NN} 2055, $\nu_{C=C}$ 1537 cm^{-1}. **IR** (solution, THF, cm^{-1}) ν_{NN} 2057, $\nu_{C=C}$ 1536 cm^{-1}. **HRMS** (ESI^+) *m/z* $[(P=NP)Ru(H)(N_2)\text{ -}H^-]^+$ calcd for $C_{20}H_{42}N_3P_2Ru$, 488.18975; found 488.18996. **Anal. Calcd** for $C_{20}H_{43}N_3P_2Ru$: C, 49.16; H, 8.87; N, 8.60. Found: C, 50.12; H, 8.61; N, 6.96.

Synthesis of (P=N=P)Ru(H)(N_2) (3). In a glovebox, **2** (14.4 mg, 0.029 mmol) was dissolved in 5 mL of benzene and added to solid $ArO^\bullet$ (15.4 mg, 0.059 mmol) resulting in a color change from purple to a dark maroon. After stirring for 17 h, the solution was dried to a sticky dark solid and taken up in 5 mL of THF. Solid KO^tBu (8.7 mg, 0.078 mmol) was added and stirred for thirty minutes to give a dark red solution. THF was removed *in vacuo* and the resulting solids extracted with pentane (3 x 2 mL) and filtered to give a red solution. Removal of pentane *in vacuo* resulted in a dark red solid which was taken up in 2mL of benzene and lyophilized to yield a red powder (13.8 mg, 96.2% yield, 96.2% pure by multinuclear NMR spectroscopy). NMR and IR spectroscopy and mass spectrometry are reported for the isolated powder. X-ray quality crystals were grown by slow evaporation of a concentrated pentane solution at 25 °C. Elemental analysis was performed on bulk powders. **^1H NMR** (600 MHz, C_6D_6): δ 7.27 (m, 2H, NC*H*), 4.20 (d, 5.4 Hz, 2H, PC*H*), 1.31 (t, 6.5 Hz, 18H, $C(CH_3)_3$), 1.19 (t, 6.4 Hz, 18H, $C(CH_3)_3$), –29.47 (t, 17.0 Hz,

1H, Ru*H*). **^{13}C{^{1}H} NMR** (152 MHz, C_6D_6) δ 163.39 (t, 10.76 Hz, N*C*H), 84.28 (t, 17.25 Hz, P*C*H), 38.04 (t, 8.52, P*C*$(CH_3)_3$), 34.46 (t, 10.44, P*C*$(CH_3)_3$), 29.39 (t, 3.64, PC(CH_3)$_3$), 29.36 (t, 3.28, PC(CH_3)$_3$). **^{31}P{^{1}H} NMR** (162 MHz, C_6D_6): δ 84.56 (s). **^{1}H-^{15}N HMBC NMR** (C_6D_6): δ 307.62 (Nα), 161.47 (N_{PNP}). **^{1}H NMR** (600 MHz, THF): δ 7.35 (m, 2H, NC*H*), 4.28 (d, 5.4 Hz, 2H, PC*H*), 1.34 (t, 6.3 Hz, 18H, C(CH_3)$_3$), 1.27 (t, 6.35 Hz, 18H, C(CH_3)$_3$), –29.84 (t, 17.0 Hz, 1H, Ru*H*). **^{31}P{^{1}H} NMR** (162 MHz, THF): δ 85.87 (s). **^{1}H-^{15}N HMBC NMR** (THF): δ 307.30 (Nα), 161.63 (N_{PNP}). **IR** (solid, cm^{-1}) ν_{NN} 2078, $\nu_{C=C}$ 1504 cm^{-1}. **IR** (solution, THF, cm^{-1}) ν_{NN} 2072, $\nu_{C=C}$ 1522 cm^{-1} cm^{-1}. **HRMS** (ESI$^+$) *m/z* [(P=N=P)Ru(H)(N_2) +H^+]$^+$ calcd for $C_{20}H_{42}N_3P_2Ru$ 488.189198; found 488.18997. **Anal. Calcd** for $C_{20}H_{41}N_3P_2Ru$: C, 49.37; H, 8.49; N, 8.64. Found: C, 51.72; H, 8.39; N, 4.92.

Synthesis of [(H-PNP)Ru(H)(N_2)][BF_4] (4). In a glovebox, (PNP)Ru(H)(N_2) (9.5 mg, 0.0194 mmol) was dissolved in 5 mL of THF and added to [HLut][BF_4] (3.7 mg, 0.0190 mmol). The red solution quickly darkened and turned orange-brown. The mixture was stirred at 25 °C for 24 h; then the volume was reduced to 1 mL *in vacuo* and pentane (10 mL) was added, resulting in the precipitation of an orange-brown solid. The mixture was cooled to -30 °C, filtered and the insoluble orange solid was washed with pentane (3 x 2 mL). The solid was collected and dried to afford an orange-brown powder (9.4 mg, 86.2% yield, 94.8% pure by multinuclear NMR spectroscopy). NMR and IR spectroscopy and mass spectrometry are reported for the isolated powder. X-ray quality crystals were grown by vapor diffusion of pentane into a concentrated sample in acetone. Elemental analysis was performed on recrystallized material. The complex was sparingly soluble in THF and therefore NMR data is also reported in CD_2Cl_2. **^{1}H NMR** (600 MHz, THF): δ 5.05 (s, 1H, N*H*), 3.54 (m, 2H, NCH_2), 2.32 (m; 6H; NCH_2, PCH_2), 1.39 (t, 6.3 Hz, 18H, C(CH_3)$_3$), 1.35 (t, 6.2 Hz, 18H, C(CH_3)$_3$), –30.32 (t, 16.0 Hz, 1H, Ru*H*). **^{13}C{^{1}H} NMR** (151 MHz, THF) δ 57.22

(t, 4.0 Hz, N*C*H_2), 37.72 (t, 8.2 Hz, *C*(CH_3)$_3$), 36.03 (t, 9.1 Hz, *C*(CH_3)$_3$), 29.06 (t, 3.0 Hz, C(*C*H_3)$_3$), 28.43 (t, 2.5 Hz, C(*C*H_3)$_3$), 23.61 (t, 8.4 Hz, P*C*H_2). **^{31}P{^{1}H} NMR** (243 MHz, THF) δ 87.63 (s). **^{19}F{^{1}H} NMR** (376 MHz, THF) –152.42 (^{10}B*F*$_4^-$), –152.47 (^{11}B*F*$_4^-$). **^{1}H NMR** (600 MHz, CD_2Cl_2): δ 4.54 (br s, 1H, N*H*), 3.52 (m, 2H, NC*H*), 2.17 (m; 6H; NCH_2, PCH_2), 1.32 (t, 6.8 Hz, 18H, C(CH_3)$_3$), 1.28 (t, 7.1 Hz, 18H, C(CH_3)$_3$), –30.43 (t, 16.1 Hz, 1H, Ru*H*). **^{13}C{^{1}H} NMR** (151 MHz, CD_2Cl_2) δ 57.05 (t, 4.1 Hz, N*C*H_2), 37.49 (t, 8.1 Hz, *C*(CH_3)$_3$), 35.84 (t, 8.9 Hz, *C*(CH_3)$_3$), 29.09 (t, 3.0 Hz, C(*C*H_3)$_3$), 28.50 (t, 2.5 Hz, C(*C*H_3)$_3$), 23.57 (t, 8.2 Hz, P*C*H_2). **^{31}P{^{1}H} NMR** (243 MHz, CD_2Cl_2) δ 86.97 (s). **^{1}H-^{15}N HMBC NMR** (CD_2Cl_2): δ 299.90 (Nα), 36.60 (N_{PNP}). **^{1}H-^{15}N HSQC NMR** (CD_2Cl_2): δ 36.61 (N_{PNP}). **IR** (solid, cm^{-1}) ν_{NN} 2107 cm^{-1}. **IR** (solution, THF, cm^{-1}) ν_{NH} 3196, ν_{NN} 2109 cm^{-1}. **HRMS** (ESI$^+$) *m/z* [(H-PNP)Ru(H)(N_2) – BF_4^-]$^+$ calcd for $C_{20}H_{46}N_3P_2Ru$ 492.22196; found 492.22104. **Anal. Calcd** for $C_{20}H_{46}N_3BF_4P_2Ru$: C, 41.53; H, 8.02; N, 7.26. Found: C, 40.23; H, 7.17; N, 6.50.

Synthesis of [(PC=NP)Ru(H)(N_2)][BF_4] (5). In a glovebox, (P=NP)Ru(H)(N_2) (11.3 mg, 0.0232 mmol) was dissolved in 5 mL of THF and added to [HLut][BF_4] (4.3 mg, 0.0221 mmol). The purple solution quickly turned orange with an orange precipitate. The mixture was stirred at 25 °C for 24 h; then pentane (8 mL) was added, resulting in the precipitation of an orange-brown solid. The mixture was filtered and the insoluble bright orange solid was washed with pentane (3 x 2 mL). The solid was collected and dried to afford a bright orange powder (12.1 mg, 95.3 % yield, 96.4% pure by multinuclear NMR spectroscopy). NMR and IR spectroscopy and mass spectrometry are reported for the isolated powder. X-ray quality crystals were grown by vapor diffusion of pentane into a concentrated sample in acetone. The complex was sparingly soluble in THF and therefore NMR data is also reported in CD_2Cl_2. Elemental analysis was performed on bulk powders. **^{1}H NMR** (600 MHz, THF): δ 8.47 (d, 24.6 Hz, 1H, NC*H*), 4.20 (m, 1H, NCH_2),

3.50 (m, 1H, NCH_2), 3.42 (m, 1H, NCHCH_2), 3.29 (dd, 19.2 Hz, 8.6 Hz, 1H, NCHCH_2), 2.37 (m, 1H, NCH_2CH_2), 2.25 (m, 1H, NCH_2CH_2), 1.44 (d, 12.6 Hz, 9H, C(CH_3)$_3$), 1.41 (d, 12.3 Hz, 9H, C(CH_3)$_3$), 1.36 (d, 12.2 Hz, 9H, C(CH_3)$_3$), 1.32 (d, 12.5 Hz, 9H, C(CH_3)$_3$), –27.21 (br s, 1H, Ru*H*). **^{13}C{^{1}H} NMR** (151 MHz, THF): δ 180.64 (s, N*C*H), 64.87 (m, N*C*H_2), 38.58 (d, 12.8 Hz, *C*(CH_3)$_3$), 36.82 (d, 14.1 Hz, *C*(CH_3)$_3$), 36.29 (d, 15.5 Hz, *C*(CH_3)$_3$), 35.74 (d, 15.9 Hz, *C*(CH_3)$_3$), 33.92 (d, 15.0 Hz, NCH*C*H_2), 29.48 (d, 5.5 Hz, C(*C*H_3)$_3$), 29.39 (d, 4.5 Hz, C(*C*H_3)$_3$), 29.08 (d, 3.8 Hz, C(*C*H_3)$_3$), 28.69 (d, 4.7 Hz, C(*C*H_3)$_3$), 23.67 (d, 15.4 Hz, NCH_2CH_2). **^{31}P{^{1}H} NMR** (243 MHz, THF) δ 91.73 (d, 247.1 Hz), 89.71 (d, 247.2 Hz). **^{19}F{^{1}H} NMR** (565 MHz, THF) –155.30 (^{10}BF_4^-), –155.35 (^{11}BF_4^-). **^{1}H NMR** (600 MHz, CD_2Cl_2): δ 8.51 (d, 24.3 Hz, 1H, N*C*H), 4.19 (ddd, 30.5 Hz, 13.5 Hz, 6.8 Hz, 1H, NCH_2), 3.49 (m, 1H, NCH_2), 3.12 (m, 2H, NCHCH_2), 2.19 (m, 1H, NCH_2CH_2), 2.07 (m, 1H, NCH_2CH_2), 1.33 (d, 13.3 Hz, 9H, C(CH_3)$_3$), 1.33 (d, 13.4 Hz, 9H, C(CH_3)$_3$), 1.26 (d, 13.6 Hz, 9H, C(CH_3)$_3$), 1.23 (d, 12.9 Hz, 9H, C(CH_3)$_3$), –29.23 (t, 16.1 Hz 1H, Ru*H*). **^{13}C{^{1}H} NMR** (151 MHz, CD_2Cl_2) δ 179.95 (dd, 7.1 Hz, 2.7 Hz, N*C*H), 65.45 (dd, 4.7 Hz, 2.2 Hz, N*C*H_2), 38.72 (dd, 14.9 Hz, 1.4 Hz, *C*(CH_3)$_3$), 36.63 (dd, 13.1 Hz, 2.3 Hz, *C*(CH_3)$_3$), 35.66 d(d, 14.9, 3.1 Hz, *C*(CH_3)$_3$), 35.31 (dd, 13.6 Hz, 2.7 Hz, *C*(CH_3)$_3$), 33.74 (dd, 13.6 Hz, 2.7 Hz, NCH*C*H_2), 29.20 (d, 5.3 Hz, C(*C*H_3)$_3$), 28.81 (d, 4.5 Hz, C(*C*H_3)$_3$), 28.55 (d, 4.6 Hz, 2 overlapping C(*C*H_3)$_3$), 23.30 (d, 16.6 Hz, NCH_2CH_2). **^{31}P{^{1}H} NMR** (243 MHz, THF) δ 92.45 (d, 240.2 Hz), 89.51 (d, 239.9 Hz). **^{1}H-^{15}N HMBC NMR** (CD_2Cl_2): δ 294.69 (Nα), 272.03 (N_{PNP}). **IR** (solid, cm^{-1}) ν_{NN} 2113 cm^{-1}. **IR** (solution, THF, cm^{-1}) ν_{NN} 2117 cm^{-1}. **HRMS** (ESI$^+$) *m/z* [(PC=NP)Ru(H)(N_2) – N_2 – BF_4^-]$^+$ calcd for $C_{20}H_{44}N1P_2Ru$ 462.198700; found 462.19955. **Anal. Calcd** for $C_{20}H_{44}N_3BF_4P_2Ru$: C, 41.67; H, 7.69; N, 7.29. Found: C, 41.95; H, 7.30; N, 3.54.

Synthesis of [(P=N=CP)Ru(H)(N_2)][BF_4] (6). In a glovebox, [H-OEt_2][BF_4] (4.0 μL, 0.0291 mmol) was diluted in 2 mL of diethyl ether and cooled to –35 °C. The solution was then added

dropwise to solid (P=N=P)Ru(H)(N_2) (14.9 mg, 0.0307 mmol) while stirring. Upon addition, an orange solid crashed out of solution and the suspension was stirred for 5 minutes. The suspension was filtered to give a pale-yellow solution and a brown-orange solid. The solid was washed with diethyl ether (3 x 2 mL), dissolved in THF and dried to give a yellow-orange solid. The solid was further dissolved in minimal CH_2Cl_2 and precipitated with 4 mL of cold diethyl ether. The resulting yellow-orange suspension was filtered and washed with diethyl ether (3 x 2 mL) and pentane (3 x 2 mL) to give an orange solid and a yellow filtrate. The orange solid was dissolved in minimal CH_2Cl_2 and precipitated with 2 mL of pentane. Solvent was removed *in vacuo* resulting in a pale yellow-orange powder. The yellow filtrate was dried *in vacuo* and a second isolation from CH_2Cl_2 and cold diethyl ether was performed resulting in further isolation of a pale yellow-orange solid (14.2 mg total, 85.0% total yield, 95.5% pure by multinuclear NMR spectroscopy). NMR and solution IR spectroscopy and mass spectrometry are reported for the isolated powder. Solid IR spectroscopy is reported for isolated X-ray quality crystals coated in Paratone oil. X-ray quality crystals were grown by vapor diffusion of pentane into a concentrated sample in acetone. Elemental analysis was performed on bulk powders. **^{1}H NMR** (600 MHz, CD_2Cl_2): δ 8.75 (d, 26.2 Hz, 1H, NC*H*CH_2), 7.67 (dd, 32.6 Hz, 6.3 Hz, 1H, NC*H*CH), 6.46 (d, 6.0 Hz, 1H, NCHC*H*), 3.41 (m, 1H, NCHCH_2), 3.29 (dd, 20.8 Hz, 7.0 Hz, 1H, NCHCH_2), 1.35 (d, 13.6 Hz, 9H, C(CH_3)$_3$), 1.34 (d, 13.2 Hz, 9H, C(CH_3)$_3$), 1.32 (d, 13.1 Hz, 9H, C(CH_3)$_3$), 1.23 (d, 13.8 Hz, 9H, C(CH_3)$_3$), –28.94 (t, 16.6 Hz Hz 1H, Ru*H*). **^{13}C{^{1}H} NMR** (151 MHz, CD_2Cl_2) δ 184.64 (dd, 7.3 Hz, 2.0 Hz, N*C*HCH_2), 158.70 (dd, 10.9 Hz, 1.6 Hz, N*C*HCH), 124.55 (d, 24.0 Hz, NCH*C*H), 39.73 (dd, 15.5 Hz, 1.0 Hz, *C*(CH_3)$_3$), 37.44 (dd, 12.5 Hz, 1.5 Hz, *C*(CH_3)$_3$), 35.42 (dd, 15.4 Hz, 2.1 Hz, *C*(CH_3)$_3$), 34.98 (d, 16.4 Hz, NCH*C*H), 34.80 (dd, 18.3 Hz, 2.8 Hz, *C*(CH_3)$_3$), 29.79 (d, 5.6 Hz, C(*C*H_3)$_3$), 29.10 (dd, 10.7 Hz, 4.9 Hz, 3 overlapping C(*C*H_3)$_3$). **^{31}P{^{1}H} NMR** (243 MHz, THF) δ 91.40 (d,

240.4 Hz), 84.82 (d, 239.8 Hz). **^{19}F{^{1}H} NMR** (376 MHz, CD_2Cl_2) –152.46 ($^{10}BF_4^-$), –152.51 ($^{11}BF_4^-$). **^{1}H-^{15}N HMBC NMR** (CD_2Cl_2): δ 295.53 (Nα), 274.42 (N_{PNP}). **IR** (solid, cm^{-1}) ν_{NN} 2116 cm^{-1}. **IR** (solution, THF, cm^{-1}) ν_{NN} 2123, $\nu_{C=C}$ 1648 cm^{-1}. **HRMS** (ESI^+) *m/z* [(P=N=CP)Ru(H)(N_2) – H_2 – BF_4^-]$^+$ calcd for $C_{20}H_{42}N_3P_2Ru$ 486.17358; found 486.17479. **Anal. Calcd** for $C_{20}H_{42}N_3BF_4P_2Ru$: C, 41.82; H, 7.37; N, 7.32. Found: C, 38.22; H, 6.83; N, 4.25.

Synthesis of (PC=NP)Ru(H)(κ^2-O_2CAr') (7). In a glovebox, (P=NP)Ru(H)(N_2) (19.9 mg, 0.041 mmol) and [HLut][BF_4] (8.7 mg, 0.045 mmol) were dissolved in 5 mL of THF and stirred. After 15 h, the dark purple solution turned orange and sodium 4-methoxybenzoate (7.1 mg, 0.041 mmol) was added. The resulting suspension was stirred for an additional 4 hours before solvent was removed under vacuum. The resulting solids were extracted with pentane (3 x 2 mL), filtered, and dried under vacuum to yield a yellow-orange solid (23.1 mg, 97% yield, 93.7% pure by multinuclear NMR spectroscopy). NMR and IR spectroscopy and mass spectrometry are reported for the isolated powder. Elemental analysis was performed on bulk powders. **^{1}H NMR** (600 MHz, C_6D_6) δ 8.34 (d, 8.8 Hz, 2H, *o*-CC*H*), 7.10 (dd, 23.6 Hz, 1.2 Hz, 1H, NC*H*), 6.71 (d, 8.4 Hz, 2H, *m*-CHC*H*), 3.40 (m, 1H, NCH_2), 3.19 (m, 1H, NCH_2), 3.14 (s, 3H, OCH_3), 2.26 (m, 8.1 Hz, 1H, CHCH_2), 2.01 (m, 1H, CHCH_2), 1.64 (m, 1H, CH_2CH_2), 1.47 (m, 27H, C(CH_3)$_3$), 1.36 (d, 11.2 Hz, 9H, C(CH_3)$_3$), 1.24 (m, 1H, CH_2CH_2), –22.17 (dd, 21.3 Hz, 18.9 Hz, 1H, Ru*H*). **^{13}C{^{1}H} NMR** (151 MHz, C_6D_6) δ 175.44 (s, C*C*O_2), 162.29 (s, *C*OCH_3), 160.22 (d, 7.0 Hz, N*C*H), 131.28 (s, *o*-C*C*H), 130.02 (s, *C*CO_2), 113.89 (s, *m*-CH*C*H), 68.26 (d, 7.7 Hz, NCH_2), 55.18 (s, OCH_3), 37.77 (d, 5.5 Hz, *C*$(CH_3)_3$), 37.68 (d, 5.5 Hz, *C*$(CH_3)_3$).35.22 (dd, 11.6 Hz, 2.7 Hz, *C*$(CH_3)_3$), 34.96 (dd, 9.2 Hz, 3.8 Hz, *C*$(CH_3)_3$), 34.26 (d, 14.5 Hz), 34.26 (d, 14.5 Hz, CH*C*H_2), 31.60 (d, 5.4 Hz, C(*C*H_3)$_3$), 31.29 (d, 5.5 Hz, C(*C*H_3)$_3$), 31.00 (d, 5.9 Hz, C(*C*H_3)$_3$), 29.79 (d, 5.9 Hz, C(*C*H_3)$_3$), 25.05 (d, 13.3 Hz, CH_2*C*H_2). **^{31}P{^{1}H} NMR** (243 MHz, C_6D_6) δ 91.51 (d, 314.5 Hz), 86.00 (d, 314.4 Hz).

IR (solution, THF, cm^{-1}) ν 1606, 1592, 1533 cm^{-1}. **HRMS** (ESI^+) *m/z* [(PC=NP)Ru(H)(O_2CAr') + H]$^+$ calcd for $C_{28}H_{52}NO_3P_2Ru$, 614.24659; found 614.24649. **Anal. Calcd** for $C_{28}H_{51}NO_3P_2Ru$: C, 54.89; H, 8.39; N, 2.29. Found: C, 52.14; H, 7.72; N, 2.08.

Synthesis of (H-PNP)Ru(H)(κ^1-O_2CAr')(N_2) (8). In a glovebox, **4** (8.4 mg, 0.014 mmol) was suspended in 4 mL of THF to which sodium 4-methoxybenzoate (3.2 mg, 0.018 mmol) was added. The mixture was stirred for 1 h during which the sparingly soluble **4** was slowly pulled into solution to yield a pale-yellow solution. The solution was dried *in vacuo*, and extracted with pentane (5 x 2mL) and filtered to give a yellow solution that dried to a pale-yellow solid (8.1 mg, 77.0% yield, 97.3% pure by multinuclear NMR spectroscopy). NMR and IR spectroscopy and mass spectrometry are reported for the isolated powder. X-ray quality crystals were grown by slow evaporation of a concentrated diethyl ether solution at 25 °C. Elemental analysis was performed on bulk powders. **^{1}H NMR** (600 MHz, C_6D_6) δ 10.96 (s(br), 1H, N*H*), 8.53 (d, 8.6 Hz, 2H, *o*-CC*H*), 6.84 (d, 8.3 Hz, 2H, *m*-CC*H*), 3.26 (s, 3H, OCH_3), 2.82 (m, 2H, NCH_2), 1.82 (m, 2H, PCH_2), 1.68 (m, 2H, NCH_2), 1.4 (m, 2H, PCH_2), 1.30 (t, 6.3 Hz, 18H, C(CH_3)$_3$), 1.22 (t, 5.8 Hz, 18H, C(CH_3)$_3$), –18.82 (t, 20.2 Hz, 1H, Ru*H*). **^{13}C{^{1}H} NMR** (151 MHz, C_6D_6) δ 174.66 (s(br), CCO_2), 162.82 (s, *C*OCH$_3$), 132.42 (s, *o*-*C*CH), 130.51 (s, *C*CO_2), 113.98 (s, *m*-CH*C*H), 55.36 (t, 4.2 Hz, N*C*H$_2$), 55.27 (s, O*C*H$_3$), 38.61 (t, 5.4 Hz, *C*(CH$_3$)$_3$)), 37.33 (dt, 9.7 Hz, 2.7 Hz, *C*(CH$_3$)$_3$)), 30.81 (s, C(*C*H$_3$)$_3$), 30.32 (s, C(*C*H$_3$)$_3$), 25.95 (t, 5.4 Hz, P*C*H$_2$). **^{31}P{^{1}H} NMR** (243 MHz, C_6D_6) δ 82.22 (s). **^{1}H-^{15}N HMBC NMR** (C_6D_6): δ 306.90 (Nα), 23.76 (N_{PNP}). **^{1}H NMR** (600 MHz, THF) δ 10.68 (s(br), 1H, N*H*), 7.90 (d, 7.9 Hz, 2H, *o*-CC*H*), 6.83 (s, 2H, *m*-CC*H*), 3.81 (s, 3H, OCH_3), 3.16 (m, 2H, NCH_2), 2.22 (m, 2H, PCH_2), 2.11 (m, 2H, NCH_2), 1.98 (m, 2H, PCH_2), 1.45 (t, 5.9 Hz, 18H, C(CH_3)$_3$), 1.34 (t, 5.8 Hz, 18H, C(CH_3)$_3$), –18.83 (t, 20.2 Hz, 1H, Ru*H*). **^{31}P{^{1}H} NMR** (243 MHz, THF) δ 82.86 (s). **^{1}H-^{15}N HMBC NMR** (THF): δ 306.16 (Nα), 26.50 (N_{PNP}). **IR** (solid, cm^{-1}) ν_{NN}

2093 cm^{-1}. **IR** (solution, THF, cm^{-1}) ν_{NH} 3188 cm^{-1}, ν_{NN} 2095 cm^{-1}. **IR** (solution, CH_2Cl_2, cm^{-1}) ν_{NH} 3214 cm^{-1}, ν_{NN} 2096 cm^{-1}. **HRMS** (ESI^+) *m/z* [(H-PNP)Ru(H)(N_2)(O_2CAr') – (O_2CAr')$^-$]$^+$ calcd for $C_{20}H_{46}N_3P_2Ru$, 492.22105; found 492.22234. **Anal. Calcd** for $C_{28}H_{53}N_3O_3P_2Ru$: C, 52.32; H, 8.31; N, 6.54. Found: C, 52.98; H, 8.15; N, 6.07.

Supporting Information

NMR and IR spectra of new complexes, electrochemistry data, and crystallographic details (PDF)

CCDC deposition numbers: 1582272-1582278

References

(1) Allen, A. D.; Senoff, C. V. Nitrogenopentammineruthenium(II) Complexes. *Chem. Commun.* **1965**, 621–622.

(2) Harrison, D. F.; Weissberger, E.; Taube, H. Binuclear Ion Containing Nitrogen as a Bridging Group. *Science (80-.).* **1968**, *159*, 320–322.

(3) Mackay, B. A.; Fryzuk, M. D. Dinitrogen Coordination Chemistry: On the Biomimetic Borderlands. *Chem. Rev.* **2004**, *104*, 385–401.

(4) Klopsch, I.; Yuzik-Klimova, E. Y.; Schneider, S. Functionalization of N_2 by Mid to Late Transition Metals via N–N Bond Cleavage. In *Topics in Organometallic Chemistry*; 2017; pp 71–112.

(5) Shima, T.; Hou, Z. Dinitrogen Fixation by Transition Metal Hydride Complexes. In *Topics in Organometallic Chemistry*; 2017; pp 23–43.

(6) Hazari, N. Homogeneous Iron Complexes for the Conversion of Dinitrogen into Ammonia and Hydrazine. *Chem. Soc. Rev.* **2010**, *39*, 4044–4056.

(7) Shaver, M. P.; Fryzuk, M. D. Activation of Molecular Nitrogen: Coordination, Cleavage and Functionalization of N_2 Mediated By Metal Complexes. *Adv. Synth. Catal.* **2003**, *345*, 1061–1076.

(8) Holland, P. L. Metal-Dioxygen and Metal-Dinitrogen Complexes: Where Are the Electrons? *Dalton Trans.* **2010**, *39*, 5415–5425.

(9) Yandulov, D. V; Schrock, R. R. Studies Relevant to Catalytic Reduction of Dinitrogen to Ammonia by Molybdenum Triamidoamine Complexes. *Inorg. Chem.* **2005**, *44*, 1103–1117.

(10) Del Castillo, T. J.; Thompson, N. B.; Peters, J. C. A Synthetic Single-Site Fe Nitrogenase: High Turnover, Freeze-Quench ^{57} Fe Mössbauer Data, and a Hydride Resting State. *J. Am. Chem. Soc.* **2016**, *138*, 5341–5350.

(11) Rittle, J.; Peters, J. C. An Fe-N_2 Complex That Generates Hydrazine and Ammonia via Fe$^{=}$ NNH_2 : Demonstrating a Hybrid Distal-to-Alternating Pathway for N_2 Reduction. *J. Am. Chem. Soc.* **2016**, *138*, 4243–4248.

(12) Fajardo, J.; Peters, J. C. Catalytic Nitrogen-to-Ammonia Conversion by Osmium and Ruthenium Complexes. *J. Am. Chem. Soc.* **2017**, *139*, 16105–16108.

(13) Bazhenova, T. A.; Shilov, A. E. Nitrogen Fixation in Solution. *Coord. Chem. Rev.* **1995**, *144*, 69–145.

(14) Hinrichsen, S.; Broda, H.; Gradert, C.; Söncksen, L.; Tuczek, F. Recent Developments in Synthetic Nitrogen Fixation. *Annu. Reports Sect. "A" (Inorganic Chem.* **2012**, *108*, 17–47.

(15) Burford, R. J.; Fryzuk, M. D. Examining the Relationship between Coordination Mode and Reactivity of Dinitrogen. *Nat. Rev. Chem.* **2017**, *1*, 26.

(16) Bart, S. C.; Lobkovsky, E.; Chirik, P. J. Preparation and Molecular and Electronic Structures of Iron(0) Dinitrogen and Silane Complexes and Their Application to Catalytic

Hydrogenation and Hydrosilation. *J. Am. Chem. Soc.* **2004**, *126*, 13794–13807.

(17) Tondreau, A. M.; Lobkovsky, E.; Chirik, P. J. Bis(imino)pyridine Iron Complexes for Aldehyde and Ketone Hydrosilylation. *Org. Lett.* **2008**, *10*, 2789–2792.

(18) Zhang, J.; Gandelman, M.; Shimon, L. J. W.; Rozenberg, H.; Milstein, D. Electron-Rich, Bulky Ruthenium PNP-Type Complexes. Acceptorless Catalytic Alcohol Dehydrogenation. *Organometallics* **2004**, *23*, 4026–4033.

(19) Zhang, J.; Gandelman, M.; Shimon, L. J. W.; Milstein, D.; Veldman, N.; Spek, A. L.; Koten, G. van. Electron-Rich, Bulky PNN-Type Ruthenium Complexes: Synthesis, Characterization and Catalysis of Alcohol Dehydrogenation. *Dalt. Trans.* **2007**, *12*, 107–113.

(20) Amoroso, D.; Jabri, A.; Yap, G. P. A.; Gusev, D. G.; dos Santos, E. N.; Fogg, D. E. The First Ru(η3-PCP) Complexes of the Electron-Rich Pincer Ligand 1,3-Bis((dicyclohexylphosphino)methyl)benzene: Structure and Mechanism in Transfer Hydrogenation Catalysis. *Organometallics* **2004**, *23*, 4047–4054.

(21) MacInnis, M. C.; MacLean, D. F.; Lundgren, R. J.; McDonald, R.; Turculet, L. Synthesis and Reactivity of Platinum Group Metal Complexes Featuring the New Pincer-like Bis(phosphino)silyl Ligand [$\varkappa^3$-(2-$Ph_2PC_6H_4$)2SiMe] $^-$ ([PSiP]): Application in the Ruthenium-Mediated Tran. *Organometallics* **2007**, *26*, 6522–6525.

(22) Tanabe, Y.; Kuriyama, S.; Arashiba, K.; Nakajima, K.; Nishibayashi, Y. Synthesis and Reactivity of Ruthenium Complexes Bearing Arsenic-Containing Arsenic-Nitrogen-Arsenic-Type Pincer Ligand. *Organometallics* **2014**, *33*, 5295–5300.

(23) Schlögl, R. Catalytic Synthesis of Ammonia—A "Never-Ending Story"? *Angew. Chemie Int. Ed.* **2003**, *42*, 2004–2008.

(24) Schüth, F.; Palkovits, R.; Schlögl, R.; Su, D. S. Ammonia as a Possible Element in an Energy Infrastructure: Catalysts for Ammonia Decomposition. *Energy Environ. Sci.* **2012**, *5*, 6278–6289.

(25) Kunkely, H.; Vogler, A. Photolysis of Aqueous [(NH3)5Os(μ-N2)Os(NH3)5]5+: Cleavage of Dinitrogen by an Intramolecular Photoredox Reaction. *Angew. Chemie Int. Ed.* **2010**, *49*, 1591–1593.

(26) Hölscher, M.; Leitner, W. Catalytic NH_3 Synthesis Using N_2/H_2 at Molecular Transition Metal Complexes: Concepts for Lead Structure Determination Using Computational Chemistry. *Chem. - A Eur. J.* **2017**, *23*, 11992–12003.

(27) Askevold, B.; Nieto, J. T.; Tussupbayev, S.; Diefenbach, M.; Herdtweck, E.; Holthausen, M. C.; Schneider, S. Ammonia Formation by Metal–ligand Cooperative Hydrogenolysis of a Nitrido Ligand. *Nat. Chem.* **2011**, *3*, 532–537.

(28) Lindley, B. M.; Bruch, Q. J.; White, P. S.; Hasanayn, F.; Miller, A. J. M. Ammonia Synthesis from a Pincer Ruthenium Nitride via Metal–Ligand Cooperative Proton-Coupled Electron Transfer. *J. Am. Chem. Soc.* **2017**, *139*, 5305–5308.

(29) Takaoka, A.; Gerber, L. C. H.; Peters, J. C. Access to Well-Defined Ruthenium(I) and Osmium(I) Metalloradicals. *Angew. Chemie Int. Ed.* **2010**, *49*, 4088–4091.

(30) Lee, Y.; Mankad, N. P.; Peters, J. C. Triggering N_2 Uptake via Redox-Induced Expulsion of Coordinated NH_3 and N_2 Silylation at Trigonal Bipyramidal Iron. *Nat. Chem.* **2010**, *2*, 558–565.

(31) Ding, K.; Pierpont, A. W.; Brennessel, W. W.; Lukat-Rodgers, G.; Rodgers, K. R.; Cundari, T. R.; Bill, E.; Holland, P. L. Cobalt–Dinitrogen Complexes with Weakened N–N Bonds. *J. Am. Chem. Soc.* **2009**, *131*, 9471–9472.

(32) Clouston, L. J.; Bernales, V.; Carlson, R. K.; Gagliardi, L.; Lu, C. C. Bimetallic Cobalt–Dinitrogen Complexes: Impact of the Supporting Metal on N_2 Activation. *Inorg. Chem.* **2015**, *54*, 9263–9270.

(33) Heiden, Z. M.; Chen, S.; Mock, M. T.; Dougherty, W. G.; Kassel, W. S.; Rousseau, R.; Bullock, R. M. Protonation of Ferrous Dinitrogen Complexes Containing a Diphosphine Ligand with a Pendent Amine. *Inorg. Chem.* **2013**, *52*, 4026–4039.

(34) Kloek, S. M.; Heinekey, D. M.; Goldberg, K. I. C-H Bond Activation by Rhodium(I) Hydroxide and Phenoxide Complexes. *Angew. Chemie Int. Ed.* **2007**, *119*, 4820–4822.

(35) Silantyev, G. A.; Förster, M.; Schluschaß, B.; Abbenseth, J.; Würtele, C.; Volkmann, C.; Holthausen, M. C.; Schneider, S. Dinitrogen Splitting Coupled to Protonation. *Angew. Chemie Int. Ed.* **2017**, *56*, 5872–5876.

(36) Bezdek, M. J.; Guo, S.; Chirik, P. J. Terpyridine Molybdenum Dinitrogen Chemistry: Synthesis of Dinitrogen Complexes That Vary by Five Oxidation States. *Inorg. Chem.* **2016**, *55*, 3117–3127.

(37) Bowman, A. C.; Milsmann, C.; Atienza, C. C. H.; Lobkovsky, E.; Wieghardt, K.; Chirik, P. J. Synthesis and Molecular and Electronic Structures of Reduced Bis(imino)pyridine Cobalt Dinitrogen Complexes: Ligand versus Metal Reduction. *J. Am. Chem. Soc.* **2010**, *132*, 1676–1684.

(38) Tondreau, A. M.; Stieber, S. C. E.; Milsmann, C.; Lobkovsky, E.; Weyhermüller, T.; Semproni, S. P.; Chirik, P. J. Oxidation and Reduction of Bis(imino)pyridine Iron Dinitrogen Complexes: Evidence for Formation of a Chelate Trianion. *Inorg. Chem.* **2013**, *52*, 635–646.

(39) Lagaditis, P. O.; Schluschaß, B.; Demeshko, S.; Würtele, C.; Schneider, S. Square-Planar

Cobalt(III) Pincer Complex. *Inorg. Chem.* **2016**, *55*, 4529–4536.

(40) Askevold, B.; Khusniyarov, M. M.; Kroener, W.; Gieb, K.; Müller, P.; Herdtweck, E.; Heinemann, F. W.; Diefenbach, M.; Holthausen, M. C.; Vieru, V.; Chibotaru, L. F.; Schneider, S. Square-Planar Ruthenium(II) Complexes: Control of Spin State by Pincer Ligand Functionalization. *Chem. - A Eur. J.* **2015**, *21*, 579–589.

(41) Schneck, F.; Finger, M.; Tromp, M.; Schneider, S. Chemical Non-Innocence of an Aliphatic PNP Pincer Ligand. *Chem. - A Eur. J.* **2017**, *23*, 33–37.

(42) Schneider, S.; Meiners, J.; Askevold, B. Cooperative Aliphatic PNP Amido Pincer Ligands - Versatile Building Blocks for Coordination Chemistry and Catalysis. *Eur. J. Inorg. Chem.* **2012**, *2012*, 412–429.

(43) Khusnutdinova, J. R.; Milstein, D. Metal-Ligand Cooperation. *Angew. Chemie Int. Ed.* **2015**, *54*, 12236–12273.

(44) Wambach, T. C.; Fryzuk, M. D. Ruthenium Complexes Stabilized by Bidentate Enamido-Phosphine Ligands: Aspects of Cooperative H_2 Activation. *Inorg. Chem.* **2015**, *54*, 5888–5896.

(45) Lagaditis, P. O.; Lough, A. J.; Morris, R. H. Low-Valent Ene–Amido Iron Complexes for the Asymmetric Transfer Hydrogenation of Acetophenone without Base. *J. Am. Chem. Soc.* **2011**, *133*, 9662–9665.

(46) Arashiba, K.; Miyake, Y.; Nishibayashi, Y. A Molybdenum Complex Bearing PNP-Type Pincer Ligands Leads to the Catalytic Reduction of Dinitrogen into Ammonia. *Nat. Chem.* **2011**, *3*, 120–125.

(47) Scheibel, M. G.; Askevold, B.; Heinemann, F. W.; Reijerse, E. J.; De Bruin, B.; Schneider, S. Closed-Shell and Open-Shell Square-Planar Iridium Nitrido Complexes. *Nat. Chem.*

2012, *4*, 552–558.

(48) Scheibel, M. G.; Wu, Y.; Stückl, A. C.; Krause, L.; Carl, E.; Stalke, D.; de Bruin, B.; Schneider, S. Synthesis and Reactivity of a Transient, Terminal Nitrido Complex of Rhodium. *J. Am. Chem. Soc.* **2013**, *135*, 17719–17722.

(49) Kinauer, M.; Scheibel, M. G.; Abbenseth, J.; Heinemann, F. W.; Stollberg, P.; Würtele, C.; Schneider, S.; Sheldrick, G. M.; Stalke, D. $[IrCl\{N(CHCHPtBu_2)_2\}]^-$: A Versatile Source of the IrI (PNP) Pincer Platform. *Dalt. Trans.* **2014**, *43*, 4506–4513.

(50) Askevold, B.; Khusniyarov, M. M.; Herdtweck, E.; Meyer, K.; Schneider, S. A Square-Planar Ruthenium(II) Complex with a Low-Spin Configuration. *Angew. Chemie Int. Ed.* **2010**, *49*, 7566–7569.

(51) Wieder, N. L.; Gallagher, M.; Carroll, P. J.; Berry, D. H. Evidence for Ligand Non-Innocence in a Formally Ruthenium(I) Hydride Complex. *J. Am. Chem. Soc.* **2010**, *132*, 4107–4109.

(52) Major, Q.; Lough, A. J.; Gusev, D. G. Substituents Effects in POP Pincer Complexes of Ruthenium. *Organometallics* **2005**, *24*, 2492–2501.

(53) Friedrich, A.; Drees, M.; Käss, M.; Herdtweck, E.; Schneider, S. Ruthenium Complexes with Cooperative PNP-Pincer Amine, Amido, Imine, and Enamido Ligands: Facile Ligand Backbone Functionalization Processes. *Inorg. Chem.* **2010**, *49*, 5482–5494.

(54) Müller, P. Practical Suggestions for Better Crystal Structures. *Crystallogr. Rev.* **2009**, *15*, 57–83.

(55) Mason, J. Nitrogen Nuclear Magnetic Resonance Spectroscopy in Inorganic, Organometallic, and Bioinorganic Chemistry. *Chem. Rev.* **1981**, *81*, 205–227.

(56) Todd, L. J.; Wilkinson, J. R. Carbon-13 Nuclear Magnetic Resonance Spectra of Metal

Carbonyl Compounds. *J. Organomet. Chem.* **1974**, *77*, 1–25.

(57) Choi, J.-H.; Heim, L. E.; Ahrens, M.; Prechtl, M. H. G. Selective Conversion of Alcohols in Water to Carboxylic Acids by in Situ Generated Ruthenium Trans Dihydrido Carbonyl PNP Complexes. *Dalt. Trans.* **2014**, *43*, 17248–17254.

(58) Choi, J.-H.; Prechtl, M. H. G. Tuneable Hydrogenation of Nitriles into Imines or Amines with a Ruthenium Pincer Complex under Mild Conditions. *ChemCatChem* **2015**, *7*, 1023–1028.

(59) Zhang, Y.; Macintosh, A. D.; Wong, J. L.; Bielinski, E. A.; Williard, P. G.; Mercado, B. Q.; Hazari, N.; Bernskoetter, W. H. Iron Catalyzed CO 2 Hydrogenation to Formate Enhanced by Lewis Acid Co-Catalysts. *Chem. Sci.* **2015**, *6*, 4291–4299.

(60) Bielinski, E. A.; Förster, M.; Zhang, Y.; Bernskoetter, W. H.; Hazari, N.; Holthausen, M. C. Base-Free Methanol Dehydrogenation Using a Pincer-Supported Iron Compound and Lewis Acid Co-Catalyst. *ACS Catal.* **2015**, *5*, 2404–2415.

(61) Alberico, E.; Lennox, A. J. J.; Vogt, L. K.; Jiao, H.; Baumann, W.; Drexler, H.-J.; Nielsen, M.; Spannenberg, A.; Checinski, M. P.; Junge, H.; Beller, M. Unravelling the Mechanism of Basic Aqueous Methanol Dehydrogenation Catalyzed by Ru–PNP Pincer Complexes. *J. Am. Chem. Soc.* **2016**, *138*, 14890–14904.

(62) Nguyen, D. H.; Morin, Y.; Zhang, L.; Trivelli, X.; Capet, F.; Paul, S.; Desset, S.; Dumeignil, F.; Gauvin, R. M. Oxidative Transformations of Biosourced Alcohols Catalyzed by Earth-Abundant Transition Metals. *ChemCatChem* **2017**, *9*, 2652–2660.

(63) Fulmer, G. R.; Miller, A. J. M.; Sherden, N. H.; Gottlieb, H. E.; Nudelman, A.; Stoltz, B. M.; Bercaw, J. E.; Goldberg, K. I. NMR Chemical Shifts of Trace Impurities: Common Laboratory Solvents, Organics, and Gases in Deuterated Solvents Relevant to the

Organometallic Chemist. *Organometallics* **2010**, *29*, 2176–2179.

(64) Viculis, L. M.; Mack, J. J.; Mayer, O. M.; Hahn, H. T.; Kaner, R. B.; Rinzler, A. G.; Colbert, D.; Smith, K. A.; Smalley, R. E. Intercalation and Exfoliation Routes to Graphite Nanoplatelets. *J. Mater. Chem.* **2005**, *15*, 974.

(65) Manner, V. W.; Markle, T. F.; Freudenthal, J. H.; Roth, J. P.; Mayer, J. M.; Nangia, A.; Thaimattam, R.; Thalladi, V. R.; Allen, F. H. The First Crystal Structure of a Monomeric Phenoxyl Radical: 2,4,6-Tri-Tert-Butylphenoxyl Radical. *Chem. Commun.* **2008**, *272*, 256–258.

(66) Thompson, E. J.; Berben, L. A. Electrocatalytic Hydrogen Production by an Aluminum(III) Complex: Ligand-Based Proton and Electron Transfer. *Angew. Chemie Int. Ed.* **2015**, *54*, 11642–11646.

(67) Dolomanov, O. V.; Bourhis, L. J.; Gildea, R. J.; Howard, J. A. K.; Puschmann, H. OLEX2: A Complete Structure Solution, Refinement and Analysis Program. *J. Appl. Crystallogr.* **2009**, *42*, 339–341.

(68) Sheldrick, G. M. *SHELXT* – Integrated Space-Group and Crystal-Structure Determination. *Acta Crystallogr. Sect. A Found. Adv.* **2015**, *71*, 3–8.

(69) Sheldrick, G. M. Crystal Structure Refinement with SHELXL. *Acta Crystallogr. Sect. C, Struct. Chem.* **2015**, *71*, 3–8.

For Table of Contents Only

TOC GRAPHIC

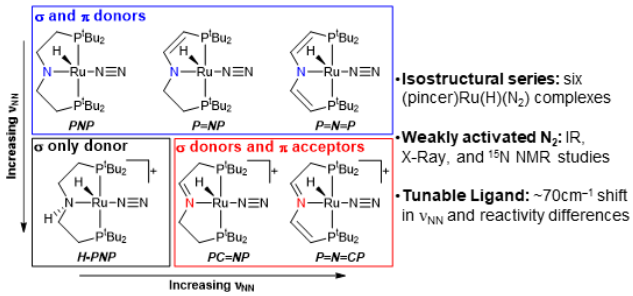

Synopsis: A family of six ruthenium hydrido dinitrogen complexes with different pincer backbone structures is presented. The N_2 ligand is retained and only weakly activated for all backbone states, with transformations in the pincer backbone from π-donating to π-accepting resulting in a shift in ν_{NN} over 70 cm^{-1}.